C.P. No. 86
(12,377, 13,735)
A.R.C. Technical Report

MINISTRY OF SUPPLY

AERONAUTICAL RESEARCH COUNCIL

CURRENT PAPERS

Pressure and Boundary Layer Measurements on a 59° Sweptback Wing at Low Speed and Comparison with High Speed Results on a 45° Swept Wing

Part I

By

Tunnel Staff of Aero Department, R.A.E.

Part II

By

G. G. Brebner, M.A.

LONDON: HER MAJESTY'S STATIONERY OFFICE

1952

Eight Shillings Net

C.P. No. 86

Report No. Aero. 2311

February, 1949.

ROYAL AIRCRAFT ESTABLISHMENT

Pressure and Boundary Layer Measurements on a 59° Sweptback Wing at Low Speed and Comparisons with High Speed Results on a 45° Swept Wing

Part I

by

Tunnel Staff of Aero. Dept.

SUMMARY

The low speed pressure distribution has been measured over a range of incidence on a 59° swept wing of symmetrical section t/c 14%, aspect ratio 3.61, taper ratio 4 to 1.

These results have been compared, using the linear perturbation theory, with those on a 45° swept wing aspect ratio 5.87 at M = 0.8. There is fairly good agreement at zero incidence but lift distribution does not appear to be predicted so well.

The results on the 59° wing show clearly the large effects of sweepback on both the pressure distribution at zero incidence and the lift distribution near the centre section of the wing. Comparisons with theoretical estimates at zero incidence show good agreement.

LIST OF CONTENTS

LIST OF TABLES

LIST OF ILLUSTRATIONS

1 Introduction

In the R.A.E. high speed tunnel, pressure measurements have been made on a tapered wing with 45° sweep back of the quarter chord line, with and without a body. A model was made for the low speed tunnel, with the angle of sweepback φ' increased so that:-

$$\tan \varphi' = \tan \varphi' / \sqrt{1 - M^2}$$

where M was taken as 0.8. This gave an angle of sweepback of 59° for the low speed model.

The purpose of the following tests was to check the linear perturbation theory by comparing the pressure distributions on the two models. The opportunity was taken to make a detailed investigation of the pressures near the centre section and at the wing tip.

2 Details of models and method

A drawing of the low speed model is given in Fig.1, and a comparison of the high and low speed models in Fig.2. Dimensions are given in Table I. The low speed model was swept back 59°, its taper ratio was 4:1, and the aspect ratio was 3.6.

On the linear perturbation theory the low speed model should have had its thickness chord ratio reduced by the factor $\sqrt{1 - M^2}$.

The pressure coefficients on the high speed model at Mach No. M should then be equal to $\left(\frac{1}{1 - M^2}\right)$ times the pressure coefficients on the low speed model. Since to the approximation of the linear theory the pressure coefficients are proportional to thickness chord ratio, the two models can be made with the same t/c and Cp on the high speed model at Mach No. M is then $\frac{1}{\sqrt{1 - M^2}}$ times the Cp on the low speed model. To avoid the difficulty of making a thin model with pressure plotting holes this latter method was used and both models have a thickness chord ratio of 14% (see Table II).

On a body of revolution however the pressure coefficients are not proportional to the thickness chord ratio; the same rule does not therefore apply and a strict comparison can only be obtained on a wing-body combination if the wing t/c and body diameter are both reduced. A body has been made however for the low speed model with a diameter/wing chord reduced to $\sqrt{1 - M^2}$ times that of the high speed model so that body effects could be studied.

For convenience its length has also been reduced.

Flush pressure holes were installed at stations D, E, F, G and H on the low speed model shown on Fig.1 and the readings were made on multitube manometers. The remaining stations A, B, C and I were explored by creeper. The tubes from the pressure holes were led from an oval hole (Fig.1) on the lower wing surface on the centre line; when the body was present they were led out at the rear of the body, but when there was no body, they passed vertically from the wing to the tunnel roof, and were faired to an oval shape. By comparing upper and lower surface readings at station D with and without the body, it appeared that the interference of these leads was negligible.

The main difficulty in using creepers on the swept back wing lay in aligning the tube along the direction of flow. In one position readings were taken with the creeper

(a) in the correct direction

(b) inclined 5°. Error found to be $\Delta/\frac{1}{2}\rho V^2 = -0.006$

(c) " 10°. " " " " " " $= -0.025$.

The direction was found by fixing silk threads at the required positions, and the accuracy should be within 5°.

The creeper readings were compared directly against flush hole readings in five positions. The creeper readings were too positive by amounts varying from 0.005 to 0.025 times $\frac{1}{2}\rho V^2$: the creeper readings have therefore been corrected by subtracting $0.015 \times \frac{1}{2}\rho V^2$. The final results are believed to be correct to $0.01 \times \frac{1}{2}\rho V^2$.

The models were tested some time after they were made and consequently the wood had warped a small amount. Readings on upper and lower surface at zero incidence were not in very good agreement and mean values have therefore had to be taken in comparing results for zero lift.

Elevons had been cut on the model, and though they were kept at 0° during the tests, some pressure readings on the elevon were affected by the gap, and cannot be used in considering wing characteristics.

3 Tests

The measurements were made in the No. 2 11½ ft tunnel during April 1948: the windspeed was 120 ft/sec giving a Reynolds number of 1.6 millions on the wing mean chord.

The following pressure measurements were made

Station	A	B	C	Body Junction	D	E	F	G	H	I
Percentage of semispan	0	2.2	6.6	9.0	12.3	24.6	39.4	68.9	93.5	98.4
α No Body	0	0	0		0	0	0			
	-	-	-		2.1	2.1	2.1			
	4.2	4.2	-		4.2	4.2	4.2			
	-	-	-		6.3	6.3	6.3			
	8.4	-	-		8.4	8.4	8.4			
α With Body				0	0	0	0	0	0	0
				-	2.1	2.1	2.1	2.1	2.1	-
				4.2	4.2	4.2	4.2	4.2	4.2	4.2
				-	6.3	6.3	6.3	6.3	6.3	-
				-	8.4	8.4	8.4	8.4	8.4	-

Sections G, H, I are beyond the influence of the body, so that the results apply both with and without body.

In addition to the pressure measurements, lift, drag and pitching moments were measured on the balance for the wing plus body, at the same five values of the incidence.

The pressure measurements will be found in Tables V-XVI and Figures 3-10. In Figures 11 and 12 they are plotted in the form of isobars. Lift and centre of pressure distributions are then given, followed in Figures 17-21 by a comparison of these tests with the M = 0.8 tests on the 45° wing.

4 Results

4.1 Low speed data

The pressure distributions at various chordwise sections along the wing are given for zero incidence in Fig.3 (wing alone) and Fig.5 (wing and body). Fig.4 shows a comparison with calculated pressure distributions. At section F (at 0.39 $b/2$, which should therefore be unaffected by the special conditions at the centre line and tip), the pressure distribution has been calculated as for an infinite yawed wing, using at any point the thickness distribution of the section normal to the local sweepback. This gives reasonable agreement with the experimental results. At the centre line of the wing without body, the calculation follows the method of Ref.2 for an infinite aspect ratio wing if the local sweepback at any point is used. The agreement with experiment is not quite so good as on an untapered wing and a more refined method of allowing for taper ratio is needed.

The large effect of the body on the pressure distribution near the wing body junction can also be seen from Fig.4. If the body had a large depth relative to the wing thickness, the pressure distribution near the side of the body would be expected to resemble that near the centre section of the wing without body. In this case, the body depth is only 1.43 times the wing thickness and the intersection of the body and wing shows a shape with a "waist". This has the effect of reducing the velocity over the region where the wing is thick as shown in Fig.4. Further tests on body effects have been made on other models and will be discussed in more detail in a later report.

The spanwise spread of the effect of the centre section is shown in Fig.6 where the pressures at various percentages of the chord are plotted against the y co-ordinate divided by the local chord. On the wing alone the interference effect is small by 0.4 y/c; with this body 0.6 to 0.7 y/c must be reached for a similar result. The theoretical spread of the centre section effect for a wing with a biconvex section (Ref.1) is in close agreement with these results on the wing alone.

The chordwise pressure distributions at $\alpha = 4.2°$ are shown in Figs. 7, 8 and the chordwise lift distribution in Figs.9,10. For sections F and G, midway between the centre section and tip the shape of the chordwise lift distribution agrees fairly well with that calculated for a two-dimensional yawed wing (Figs.9,10), but over the inboard sections there is an induced camber effect giving a loss of lift and backward movement of the centre of pressure compared with an unswept wing (Figs. 14,15,16). Outboard near the tip the induced camber effect is of opposite sign but generally smaller. The curves of local lift coefficient against incidence (Fig.13) show a very early stall for the tip sections; C_L max at section H (at 0.95 $b/2$) is apparently only just over 0.3.

Adding the body increases the lift near the wing root due to the local upwash round the body (Figs.14,15). It should be noted that the effects of the centre section on the lift distribution spread out much further than at zero incidence.

It is hoped to make a detailed comparison of these results with the theoretical lift distribution later.

4.2 Comparison of high speed and low speed results

Four stations were available on the 45° swept wing tested at M = 0.8, at the following distances from the centre line: $2y/b$ = 0.15, 0.39, 0.69 and 0.94. The results at zero incidence are compared in Figs. 17,18 with stations F, G and H and an interpolated result at $2y/b$ = 0.15 on the 59° wing. Particularly on the 59° wing, the agreement between upper and lower surface is not good, but the comparison between the curves which represent the mean values for upper and lower surfaces is satisfactory. The curves for M = 0.4 on the 45° wing show the magnitude of the Mach No. effect and it can be seen that the analogous low speed model gives the compressibility effect fairly accurately.

With body on, the agreement is not so good for the reasons which have already been discussed in paragraph 2.

The integrated lift distributions and centres of pressures are compared in Fig.20. Here the agreement is not quite so good. To eliminate the effect of any possible twist in the wing the difference in lift between α = 0° and α = 4.2° has been plotted. From a comparison of the results on the 45° wing at M = 0.8 and 0.6 (the lowest Mach No. for which results are available) the 59° wing appears to give an over-estimate of the compressibility effect over most of the wing. Detailed comparison of the chordwise loadings due to incidence (Fig.21) does not suggest any obvious reason for this. It is possible that the kinks in the curves for the 45° wing at 0.4c on the two inboard sections may be due to the presence of a shock wave, but it is difficult without a more detailed chordwise pressure distribution to see exactly when the shock wave starts. If a shock wave is present it would account for the failure of the 59° wing to predict the lift distribution on the 45° wing. Near the tip differences might be expected since the boundary layer is thick and has a large effect on the local lift.

5 Conclusions

(a) The experimental low speed pressure distributions on the 59° swept back wing are in reasonable agreement with theory at zero incidence. A body causes a reduction of the maximum velocity at the wing body root due to effect of the 'waist' produced by the intersection of the wing and body.

(b) There are very large changes in the chordwise lift loading along the span of a highly swept wing; comparisons with theory will be made later.

(c) The comparison of the low speed results on the 59° wing (multiplied by $\frac{1}{\sqrt{1 - 0.8^2}}$ in accordance with the linear perturbation theory), with those on a 45° swept wing at M = 0.8 shows reasonably good agreement in general, better on the pressure distribution at zero incidence than on the lift distribution.

REFERENCES

Ref. No.	Author	Title, etc.
1	S. Neumark	Velocity distribution on straight and swept back wings of small thickness and infinite aspect ratio at zero incidence. R. & M. 2713. May, 1947.
2	D. Küchemann	Wing Junction, fuselage and nacelles for swept back wings. (to be published) A.R.C. 11,035.

TABLE I

Model data

	Low speed tunnel model	High speed tunnel model
Angle of sweep of quarter chord line φ	59°	45°
tan φ	$1/\sqrt{1 - 0.8^2}$	1
Profile section H.S.6 scaled up to t/c	0.14	0.14
Taper ratio	4:1	4:1
Aspect ratio	3.61	5.87
Semi span b/2	45.72"	55.06"
Centre chord	41.14"	30"
Tip chord	10.28"	7.5"
Mean chord $\bar{c}$	25.36"	18.77"
Area	16.10 sq.ft	14.36 sq.ft
Body diameter D	8.22"	9.84"
Body length L	100"	91.5"
Ratio of body diameter to wing thickness at centre section	1.43	2.34
Thickness ratio of body D/L	0.082	0.107

TABLE II

Co-ordinates of the Profile Section of Both Models

x/c	z/c
0	0
0.0125	0.0192
0.025	0.0268
0.05	0.0372
0.1	0.0505
0.2	0.0648
0.3	0.0700
0.4	0.0672
0.5	0.0597
0.6	0.0494
0.7	0.0375
0.8	0.0250
0.9	0.0125
1.0	0

TABLE III

Co-ordinates of the Body of the Low Speed Tunnel Model

The body consisted of a cylinder with front and rear fairings. The cylindrical part extended from x/L = 0.194 to 0.787.

FRONT PART	
x/L	r/L
0	0
0.0084	0.0133
0.0167	0.0183
0.0251	0.0219
0.0335	0.0248
0.050	0.0292
0.067	0.0325
0.084	0.0350
0.100	0.0369
0.117	0.0384
0.134	0.0397
0.151	0.0403
0.167	0.0408
0.184	0.0410
0.194	0.0411

REAR PART	
x/L	r/L
0.787	0.0411
0.803	0.0408
0.820	0.0400
0.837	0.0386
0.853	0.0369
0.870	0.0348
0.887	0.0325
0.904	0.0298
0.921	0.0269
0.937	0.0238
0.954	0.0205
0.971	0.0170
0.987	0.0132
0.996	0.0111
1.000	0.0101

TABLE IV

Details of pressure plotting stations

Section	y (")	$\frac{y}{b/2}$	$\frac{y}{c}$	$\frac{b/2 - y}{c}$	$\frac{c}{\bar{c}}$
A*	0	0	0		1.622
B*	1	0.022	0.025		1.595
C*	3	0.066	0.077		1.541
Wing Body Junction*	4.11	0.090	0.107		1.511
D	5.62	0.123	0.151		1.470
E	11.25	0.246	0.336		1.318
F	18.0	0.394	0.625	0.963	1.136
G	31.5	0.689	1.612	0.728	0.771
H	42.75	0.935		0.251	0.466
I*	45.0	0.984		0.070	0.405

* Measurements of these stations made by creeper.

TABLE V

Pressure Coefficient at Centre Section A

UPPER SURFACE			
$\frac{x}{c}$ \ α	0°	4.2°	8.4°
0.038	0.29	0.19	0.03
0.083	0.06	-0.04	-0.18
0.130	-0.02	-0.13	-0.24
0.227	-0.12	-0.21	-0.30
0.323	-0.20	-0.28	-0.36
0.420	-0.24	-0.31	-0.39
0.517	-0.23	-0.29	-0.36
0.614	-0.20	-0.25	-0.31
0.710	-0.16	-0.21	-0.25
0.807	-0.12	-0.15	-0.19
0.904	-0.07	-0.09	-0.11

LOWER SURFACE			
$\frac{x}{c}$ \ α	0°	4.2°	8.4°
0.038	0.29	0.40	0.52
0.083	0.08	0.19	0.31
0.130	-0.01	0.10	0.21
0.227	-0.13	-0.02	0.10
0.323	-0.19	-0.09	0.01
0.420	-0.23	-0.13	-0.04
0.517	-0.22	-0.14	-0.05
0.614	-0.20	-0.12	-0.04
0.710	-0.15	-0.09	-0.02
0.807	-0.11	-0.06	0.00
0.904	-0.05	-0.02	0.03

TABLE VI

Pressure Coefficient without Body at Sections B and C

SECTION B AT $y = 0.022\ b/2$

$\frac{x}{c}$ \ α	UPPER SURFACE		LOWER SURFACE	
	0°	4.2°	0°	4.2°
0.023	0.14	0.02	0.15	0.22
0.114	-0.05	-0.19	-0.06	0.05
0.211	-0.15	-0.26	-0.16	-0.04
0.310	-0.22	-0.32	-	-0.08
0.409	-0.23	-0.31	-0.24	-0.14
0.508	-0.22	-0.29	-0.23	-0.15
0.705	-0.14	-0.19	-0.16	-0.09
0.902	-0.05	-0.07	-0.04	0.00

SECTION C AT $y = 0.066\ b/2$
$\alpha = 0$

$\frac{x}{c}$	UPPER	LOWER
0.038	0.02	0.01
0.086	-0.08	-0.10
0.185	-0.19	-0.19
0.287	-0.25	-0.23
0.389	-0.24	-0.25
0.491	-0.23	-0.23
0.695	-0.13	-0.15

TABLE VII

Pressure Coefficient Without Body

SECTION D AT $y = 0.123\ b/2$

UPPER SURFACE					
x/c \ α	0°	2.1°	4.2°	6.3°	8.4°
0.015	0.06	-0.04	-0.17	-0.30	-0.46
0.03	-0.02	-0.13	-0.25	-0.38	-0.53
0.05	-0.11	-0.22	-0.33	-0.45	-0.60
0.08	-0.16	-0.26	-0.36	-0.47	-0.59
0.14	-0.22	-0.30	-0.38	-0.46	-0.56
0.20	-	-	-	-	-
0.30	-0.27	-0.33	-0.39	-0.44	-0.48
0.43	-0.24	-0.28	-0.32	-0.35	-0.39
0.56	-0.17	-0.19	-0.22	-0.24	-0.27
0.69	-0.09	-0.11	-0.12	-0.14	-0.16
0.82	-0.03	-0.04	-0.04	-0.05	-0.06
0.95	0.05	0.05	0.06	0.07	0.06

LOWER SURFACE					
x/c \ α	0°	2.1°	4.2°	6.3°	8.4°
0.015	0.09	0.16	0.20	0.23	0.23
0.03	-0.01	0.09	0.15	0.20	0.23
0.05	-0.10	0.00	0.07	0.14	0.19
0.08	-0.16	-0.07	0.00	0.07	0.13
0.11	-0.25	-0.16	-0.09	-0.03	0.04
0.20	-0.27	-0.20	-0.13	-0.07	-0.01
0.30	-0.28	-0.21	-0.16	-0.10	-0.04
0.43	-0.25	-0.19	-0.15	-0.10	-0.06
0.56	-0.18	-0.14	-0.11	-0.07	-0.03
0.69	-0.11	-0.08	-0.05	-0.02	0.01
0.82	-0.03	-0.01	0.01	0.03	0.05
0.95	0.05	0.06	0.06	0.07	0.07

TABLE VIII

Pressure Coefficient without Body

SECTION E AT $y = 0.246\ b/2$

UPPER SURFACE					
$\frac{x}{c}$ \ α	0°	2.1°	4.2°	6.3°	8.4°
0.015	0.04	-0.09	-0.25	-0.43	-0.66
0.03	-0.04	-0.18	-0.34	-0.51	-0.72
0.05	-0.14	-0.28	-0.44	-0.60	-0.80
0.08	-0.23	-0.36	-0.50	-0.65	-0.82
0.14	-0.26	-0.36	-0.48	-0.59	-0.70
0.20	-0.30	-0.38	-0.47	-0.56	-0.65
0.30	-0.29	-0.35	-0.42	-0.48	-0.55
0.43	-0.24	-0.28	-0.32	-0.36	-0.40
0.56	-0.14	-0.17	-0.19	-0.22	-0.24
0.69	-0.06	-0.08	-0.09	-0.10	-0.11
0.82	-0.02	-0.02	-0.02	-0.02	-0.02
0.95	0.05	0.05	0.06	0.06	0.05

LOWER SURFACE					
$\frac{x}{c}$ \ α	0°	2.1°	4.2°	6.3°	8.4°
0.015	0.02	0.12	0.18	0.20	0.19
0.03	-0.07	0.05	0.13	0.19	0.21
0.05	-0.15	-0.03	0.07	0.14	0.20
0.08	-0.20	-0.09	0.01	0.09	0.15
0.14	-0.24	-0.14	-0.06	0.02	0.10
0.20	-0.24	-0.15	-0.08	-0.01	0.06
0.30	-0.27	-0.20	-0.13	-0.07	-0.01
0.43	-	-	-	-	-
0.56	-0.16	-0.12	-0.08	-0.05	-0.01
0.69	-0.08	-0.06	-0.03	-0.01	0.02
0.82	-0.02	0.00	0.01	0.03	0.04
0.95	0.06	0.06	0.06	0.06	0.06

TABLE IX

Pressure Coefficient Without Body

SECTION F AT $y = 0.394\ b/2$

UPPER SURFACE					
$\frac{x}{c}$ \ α	0°	2.1°	4.2°	6.3°	8.4°
0.015	0.06	-0.11	-	-0.53	-0.83
0.03	-	-	-	-	-
0.05	-0.14	-0.30	-	-0.71	-0.95
0.08	-0.24	-0.39	-	-0.75	-0.95
0.14	-0.28	-0.41	-	-0.70	-0.86
0.20	-0.29	-0.40	-	-0.63	-0.79
0.30	-0.27	-0.34	-	-0.46	-0.55
0.43	-0.23	-0.27	-	-0.36	-0.40
0.56	-0.11	-0.16	-	-0.20	-0.22
0.69	-0.07	-0.08	-	-0.09	-0.10
0.82	-0.01	-0.02	-	-0.01	-0.01
0.95	0.06	0.06	-	0.07	0.05

LOWER SURFACE					
$\frac{x}{c}$ \ α	0°	2.1°	4.2°	6.3°	8.4°
0.015	0.05	0.15	-	0.19	0.13
0.03	-0.07	0.07	-	0.21	0.21
0.05	-0.17	0.02	-	0.17	0.22
0.08	-0.22	-0.08	-	0.11	0.18
0.14	-0.26	-0.14	-	0.04	0.12
0.20	-0.26	-0.15	-	0.00	0.08
0.30	-0.28	-0.19	-	-0.05	0.02
0.43	-0.27	-0.20	-	-0.08	-0.01
0.56	-0.16	-0.12	-	-0.05	-0.01
0.69	-0.05	-0.05	-	0.01	0.03
0.82	0.01	0.01	-	0.02	0.03
0.95	0.07	0.05	-	0.04	0.04

TABLE X

Pressure Coefficient at Wing Body Junction

	UPPER SURFACE		LOWER SURFACE	
$\frac{x}{c}$ \ α	0°	4.2°	0°	4.2°
0.05	0.06	-0.12	0.09	0.23
0.1	-0.04	-0.18	-0.02	0.11
0.2	-0.11	-0.22	-0.09	0.02
0.3	-0.15	-0.24	-0.13	-0.03
0.4	-0.17	-0.25	-0.15	-0.07
0.5	-0.17	-0.24	-0.15	-0.07
0.6	-0.15	-0.20	-0.15	-0.08
0.7	-0.14	-0.18	-0.13	-0.07
0.8	-0.11	-0.14	-0.11	-0.05
0.9	-0.08	-0.10	-0.07	-0.02

TABLE XI

Pressure Coefficient With Body

SECTION D AT y = 0.123 $^{b}/_{2}$

UPPER SURFACE					
$\frac{x}{c}$ \ α	0°	2.1°	4.2°	6.3°	8.4°
0.015	0.17	0.07	-0.06	-0.21	-0.38
0.03	0.09	-0.02	-0.15	-0.29	-0.44
0.05	0.00	-0.11	-0.23	-0.36	-0.50
0.08	-0.07	-0.17	-0.27	-0.38	-0.49
0.14	-0.13	-0.20	-0.29	-0.37	-0.45
0.20	-0.15	-0.22	-0.29	-0.35	-0.41
0.30	-0.20	-0.25	-0.30	-0.35	-0.40
0.43	-0.18	-0.22	-0.26	-0.30	-0.33
0.56	-0.14	-0.17	-0.20	-0.23	-0.27
0.69	-0.10	-0.12	-0.15	-0.17	-0.20
0.82	-0.07	-0.09	-0.11	-0.12	-0.13
0.95	0.01	0.00	0.00	0.00	0.00

LOWER SURFACE					
$\frac{x}{c}$ \ α	0°	2.1°	4.2°	6.3°	8.4°
0.015	0.18	0.25	0.30	0.32	0.33
0.03	0.08	0.17	0.24	0.29	0.33
0.05	0.00	0.09	0.17	0.24	0.29
0.08	-0.05	0.03	0.11	0.18	0.24
0.14	-0.08	-0.01	0.06	0.12	0.18
0.20	-0.13	-0.06	0.00	0.06	0.12
0.30	-0.16	-0.11	-0.05	0.00	0.05
0.43	-0.17	-0.13	-0.08	-0.03	0.01
0.56	-0.14	-0.10	-0.06	-0.03	0.01
0.69	-0.10	-0.07	-0.04	-0.01	0.03
0.82	-0.06	-0.04	-0.02	0.01	0.04
0.95	0.01	0.02	0.03	0.05	0.06

TABLE XII

Pressure Coefficient With Body

SECTION E AT $y = 0.246\ b/2$

UPPER SURFACE					
$\frac{x}{c}$ \ α	0°	2.1°	4.2°	6.3°	8.4°
0.015	0.07	-0.05	-0.22	-0.41	-0.64
0.03	-0.01	-	-0.30	-0.48	-0.69
0.05	-0.10	-0.24	-0.40	-0.57	-0.77
0.08	-0.19	-0.31	-0.46	-0.61	-0.79
0.14	-0.22	-0.32	-0.43	-0.54	-0.66
0.20	-0.25	-0.34	-0.43	-0.52	-0.61
0.30	-0.26	-0.32	-0.39	-0.46	-0.53
0.43	-0.22	-0.27	-0.31	-0.35	-0.39
0.56	-0.14	-0.17	-0.20	-0.23	-0.26
0.69	-0.08	-0.10	-0.11	-0.13	-0.16
0.82	-0.03	-0.05	-0.04	-0.05	-0.08
0.95	0.03	0.03	0.03	0.03	0.00

LOWER SURFACE					
$\frac{x}{c}$ \ α	0°	2.1°	4.2°	6.3°	8.4°
0.015	0.06	0.16	0.21	0.23	0.20
0.03	-0.02	0.09	0.17	0.22	0.23
0.05	-0.10	0.02	0.11	0.19	0.23
0.08	-	-	-	-	-
0.14	-0.20	-0.10	-0.02	0.05	0.12
0.20	-0.16	-0.08	-0.01	0.06	0.12
0.30	-0.23	-0.16	-0.09	-0.03	0.03
0.43	-0.22	-0.16	-0.11	-0.06	-0.01
0.56	-0.15	-0.11	-0.07	-0.03	0.01
0.69	-0.09	-0.06	-0.03	0.00	0.03
0.82	-0.05	-0.01	0.00	0.02	0.04
0.95	0.05	0.05	0.05	0.06	0.06

TABLE XIII

Pressure Coefficient With Body

SECTION F AT y = 0.394 b/2

UPPER SURFACE					
x/c \ α	0°	2.1°	4.2°	6.3°	8.4°
0.015	0.05	-0.10	-0.31	-0.57	-0.86
0.03	-0.05	-0.22	-0.43	-0.68	-0.96
0.05	-0.13	-0.30	-0.50	-0.71	-0.96
0.08	-0.23	-0.39	-0.56	-0.74	-0.94
0.14	-0.28	-0.41	-0.55	-0.69	-0.85
0.20	-0.29	-0.40	-0.51	-0.62	-0.74
0.30	-0.27	-0.34	-0.41	-0.49	-0.56
0.43	-0.23	-0.28	-0.32	-0.36	-0.40
0.56	-0.14	-0.17	-0.19	-0.21	-0.22
0.69	-0.07	-0.07	-0.09	-0.10	-0.12
0.82	-	-	-	-	-
0.95	0.06	0.06	0.05	0.03	-0.02

LOWER SURFACE					
x/c \ α	0°	2.1°	4 2°	6.3°	8.4°
0.015	0.07	0.16	0.20	0.19	0.12
0.03	-0.04	0.08	0.17	0.21	0.20
0.05	-0.14	0.01	0.11	0.18	0.22
0.08	-0.19	-0.05	0.06	0.14	0.20
0.14	-0.23	-0.12	-0.02	0.07	0.14
0.20	-0.22	-0.12	-0.04	0.04	0.10
0.30	-0.27	-0.18	-0.10	-0.03	0.04
0.43	-0.25	-0.19	-0.12	-0.06	0.00
0.56	-0.16	-0.13	-0.09	-0.04	-0.01
0.69	-0.06	-0.05	-0.03	-0.01	0.02
0.82	-0.01	0.00	0.00	0.01	0.02
0.95	0.05	0.04	0.03	0.02	0.01

TABLE XIV

Pressure Coefficient with Body

SECTION G AT y = 0.689 b/2

UPPER SURFACE					
x/c \ α	0°	2.1°	4.2°	6.3°	8.4°
0.015	0.09	-0.08	-0.32	-0.62	-0.96
0.03	-0.02	-0.21	-0.44	-0.74	-1.07
0.05	-0.10	-0.30	-0.54	-0.80	-1.09
0.08	-0.20	-0.40	-0.60	-0.82	-1.06
0.14	-0.30	-0.46	-0.63	-0.80	-0.96
0.20	-0.28	-0.44	-0.56	-0.64	-0.74
0.30	-0.23	-0.34	-0.38	-0.45	-0.48
0.43	-0.20	-0.24	-0.29	-0.30	-0.26
0.56	-0.12	-0.14	-0.16	-0.12	-0.10
0.72	-0.03	-0.04	-0.02	-0.02	-0.08
0.75	0.00	0.00	0.01	0.00	-0.07
0.80	0.01	0.02	0.03	0.00	-0.08
0.90	0.07	0.07	0.06	0.02	-0.09

LOWER SURFACE					
x/c \ α	0°	2.1°	4.2°	6.3°	8.4°
0.015	0.05	0.18	0.23	0.22	0.14
0.03	-0.05	0.10	0.20	0.23	0.20
0.05	-0.18	-0.01	0.11	0.19	0.22
0.08	-0.23	-0.07	0.05	0.14	0.20
0.14	-0.24	-0.12	-0.01	0.08	0.15
0.20	-0.24	-0.14	-0.05	0.02	0.10
0.30	-0.22	-0.14	-0.07	-0.01	0.05
0.43	-0.21	-0.15	-0.11	-0.06	-0.02
0.56	-0.12	-0.10	-0.06	-0.04	-0.02
0.72	-0.03	-0.02	-0.01	-0.01	0.00
0.75	-0.01	0.00	0.00	0.00	0.00
0.78	0.00	0.00	0.00	0.00	0.00
0.85	0.03	0.02	0.01	0.00	-0.01
0.95	0.08	0.07	0.05	0.02	-0.03

TABLE XV

Pressure Coefficient With Body

SECTION H AT y = 0.935 b/2

UPPER SURFACE					
x/c \ α	0°	2.1°	4.2°	6.3°	8.4°
0.015	0.09	-0.13	-0.42	-0.74	-1.06
0.03	0.02	-0.22	-0.50	-0.80	-1.07
0.05	-0.06	-0.30	-0.57	-0.84	-1.07
0.08	-0.16	-0.39	-0.62	-0.84	-1.01
0.14	-0.26	-0.45	-0.63	-0.78	-0.88
0.20	-0.27	-0.42	-0.56	-0.70	-0.78
0.30	-0.24	-0.34	-0.47	-0.44	-0.42
0.43	-0.19	-0.26	-0.27	-0.28	-0.17
0.56	-0.09	-0.10	-0.11	-0.09	-0.02
0.72	-0.06	-0.05	-0.04	0.02	0.02
0.75	-0.01	-0.01	0.00	0.04	0.02
0.80	0.02	0.02	0.03	0.06	0.02
0.90	0.10	0.10	0.10	0.09	0.02

LOWER SURFACE					
x/c \ α	0°	2.1°	4.2°	6.3°	8.4°
0.015	0.02	0.16	0.20	0.15	0.05
0.03	-0.07	0.10	0.19	0.20	0.17
0.05	-	-	-	-	-
0.08	-0.19	-0.04	0.08	0.16	0.20
0.14	-0.25	-0.11	0.00	0.08	0.14
0.20	-0.25	-0.14	-0.04	0.03	0.08
0.30	-0.22	-0.15	-0.08	-0.03	0.00
0.43	-0.18	-0.14	-0.10	-0.07	-0.05
0.56	-0.13	-0.10	-0.09	-0.07	-0.07
0.72	0.00	-0.01	-0.02	-0.02	-0.05
0.75	0.02	0.00	0.00	-0.02	-0.04
0.78	0.04	0.02	0.02	0.00	-0.03
0.85	0.07	0.06	0.04	0.02	-0.02

TABLE XV

Pressure Coefficient with Body

SECTION I AT y = 0.904 b/2

	UPPER SURFACE		LOWER SURFACE	
$\frac{x}{c}$ \ α	0^o	4.2^o	0^o	4.2^o
0.038	-0.08	-0.49	-0.16	0.09
0.130	-0.23	-0.53	-0.28	-0.07
0.225	-0.29	-0.47	-0.29	-0.16
0.322	-0.23	-0.31	-0.25	-0.18
0.419	-0.14	-0.20	-0.16	-0.15
0.516	-0.07	-0.10	-0.09	-0.09
0.613	-0.03	-0.07	-0.03	-0.07
0.807	0.07	-0.13	0.07	-0.11

TABLE XVII

Local Lift Coefficients From Pressure Distributions

WITHOUT BODY

α	C_L AT SECTION				
	A 0	B 0.022 b/2	D 0.123 b/2	E 0.246 b/2	F 0.394 b/2
0°	-0.006	-0.010	-0.001	0.001	-0.004
2.1°	-	-	0.083	0.101	0.108
4.2°	0.154	0.144	0.159	0.183	-
6.3°	-	-	0.235	0.280	0.310
8.4°	0.306	-	0.321	0.369	0.423

WITH BODY

α	C_L AT SECTION						
	Wing Body Junction	D 0.123 b/2	E 0.246 b/2	F 0.394 b/2	G 0.689 b/2	H 0.935 b/2	I 0.984 b/2
0°	0.014	0.013	0.013	0.003	-0.006	0.002	-0.018
2.1°	-	0.100	0.113	0.110	0.110	0.118	-
4.2°	0.169	0.189	0.204	0.228	0.211	0.223	0.137
6.3°	-	0.270	0.298	0.325	0.304	0.279	-
8.4°	-	0.353	0.401	0.434	0.390	0.301	-

TABLE XVIII

Local Pitching Moment Coefficients About The Quarter Chord Point From Pressure Distributions

WITHOUT BODY

α	C_M AT SECTION				
	A 0	B 0.022 b/2	D 0.123 b/2	E 0.246 b/2	F 0.394 b/2
0°	0.004	0.004	0.003	0.002	0.000
2.1°	-	-	-0.004	-0.001	0.002
4.2°	-0.023	-0.018	-0.008	-0.003	-
6.3°	-	-	-0.013	-0.003	0.003
8.4°	-0.044	-	-0.018	-0.007	0.002

WITH BODY

α	C_M AT SECTION						
	Wing Body Junction	D 0.123 b/2	E 0.246 b/2	F 0.394 b/2	G 0.689 b/2	H 0.935 b/2	I 0.984 b/2
0°	0.000	-0.001	0.000	0.004	0.008	-0.003	-0.001
2.1°	-	-0.008	-0.002	0.003	0.010	0.006	-
4.2°	-0.020	-0.016	-0.007	0.001	0.011	0.016	0.010
6.3°	-	-0.024	-0.012	0.000	0.017	0.030	-
8.4°	-	-0.031	-0.020	-0.006	0.016	0.042	-

TABLE XIX

Coefficients of Total Lift, Drag and Pitching Moment.

Balance Measurements.

WITH BODY

α	C_L	C_D	C_M
0°	0.001	0.0122	0.0019
2.1°	0.101	0.0125	0.0172
4.2°	0.195	0.0150	0.0340
6.3°	0.286	0.0196	0.0540
8.4°	0.373	0.0270	0.0775

Position of pitching moment axis:-

Aft of leading edge of centre line chord	46.72 in.
Below chord	1.18 in.
Aft of leading edge of standard mean chord	0.506 $\bar{c}$
Below chord	0.047 $\bar{c}$

FIG. I.

	SPANWISE POSITION OF PRESSURE POINTS AS % OF $b/2$
A	0·0
B	2 19
C	6·57
D	12·3
E	24 6
F	39 4
G	68 9
H	93 5
I	98·5

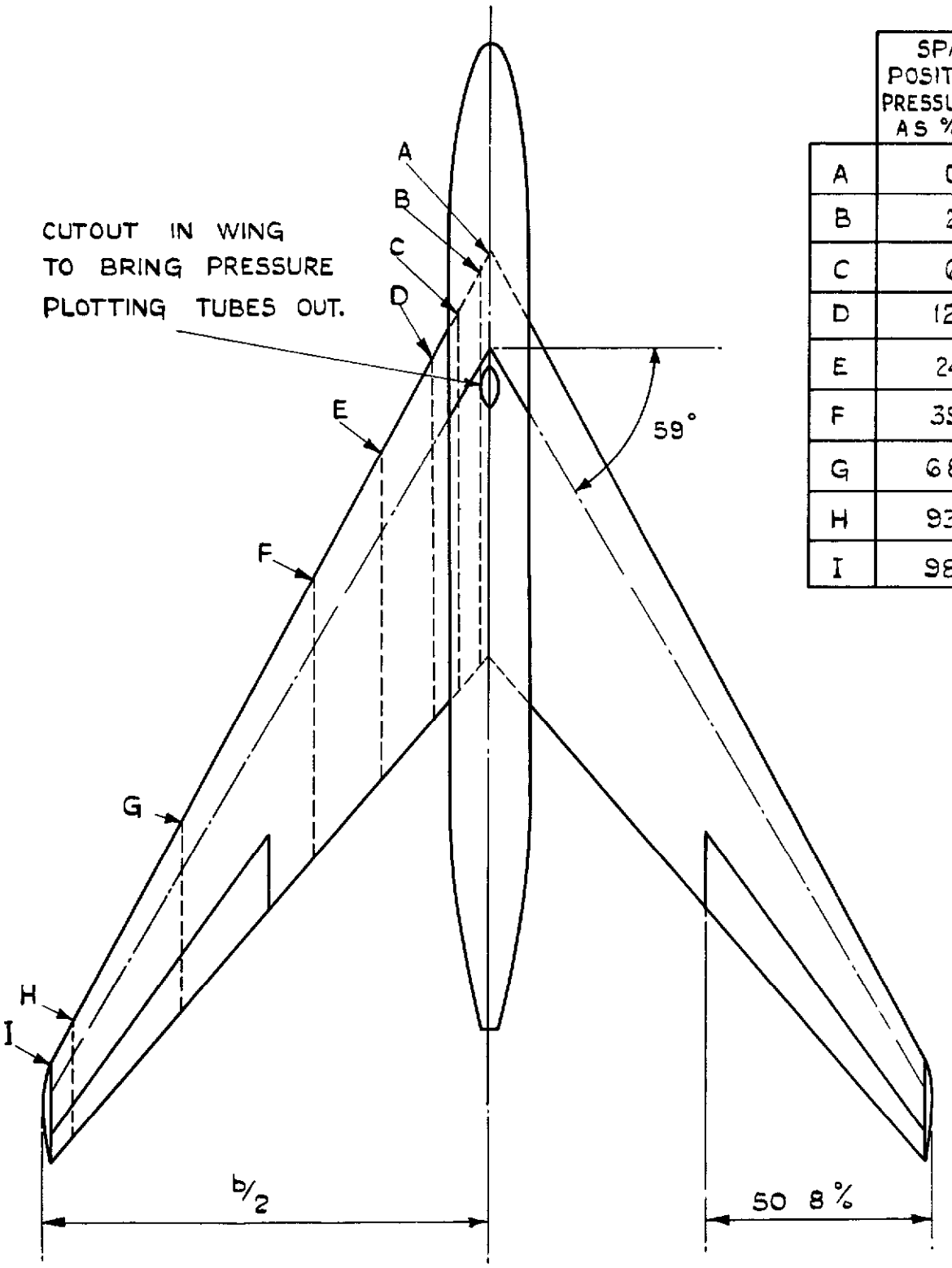

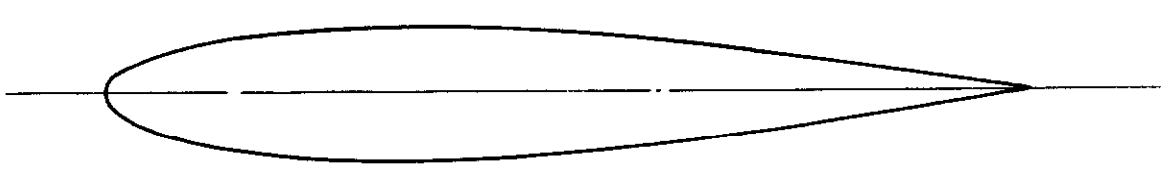

TYPICAL SECTION $t/c = 0\ 14.$

FIG. I. G.A. OF LOW SPEED MODEL

FIG. 2.

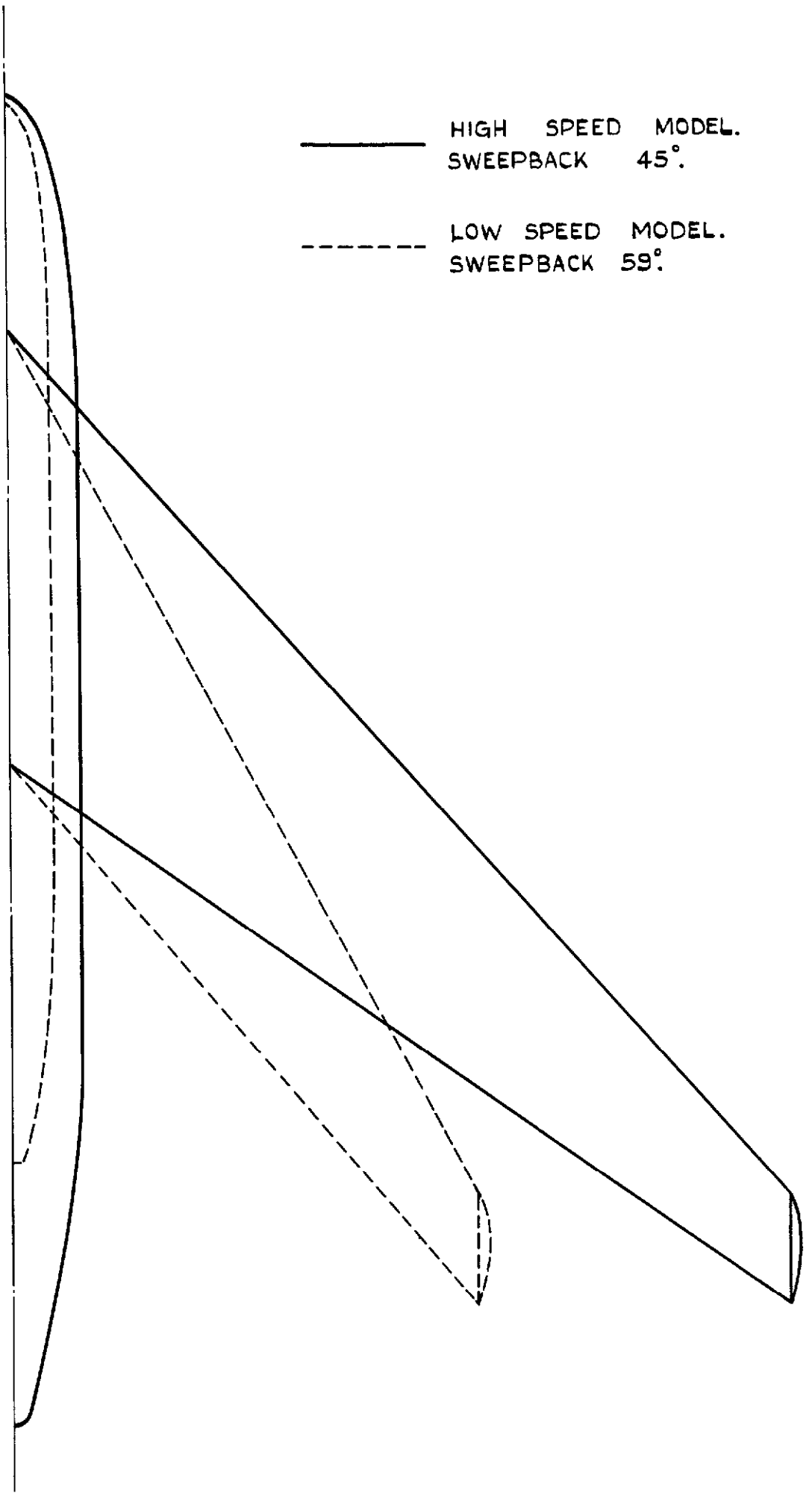

FIG. 2. COMPARISON OF HIGH SPEED AND LOW SPEED MODELS.

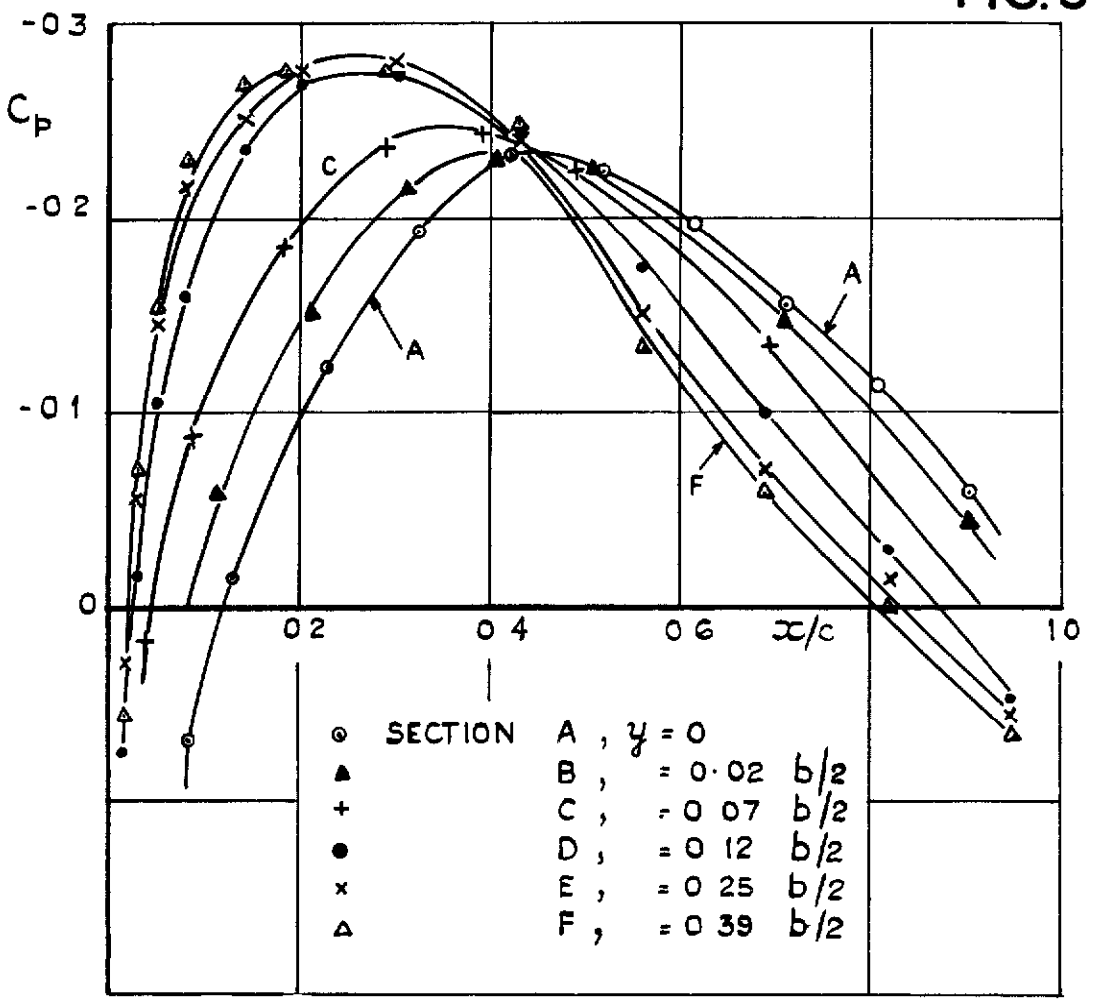

FIG. 3. PRESSURE DISTRIBUTION. 59° WING, NO BODY, $\alpha = 0$.

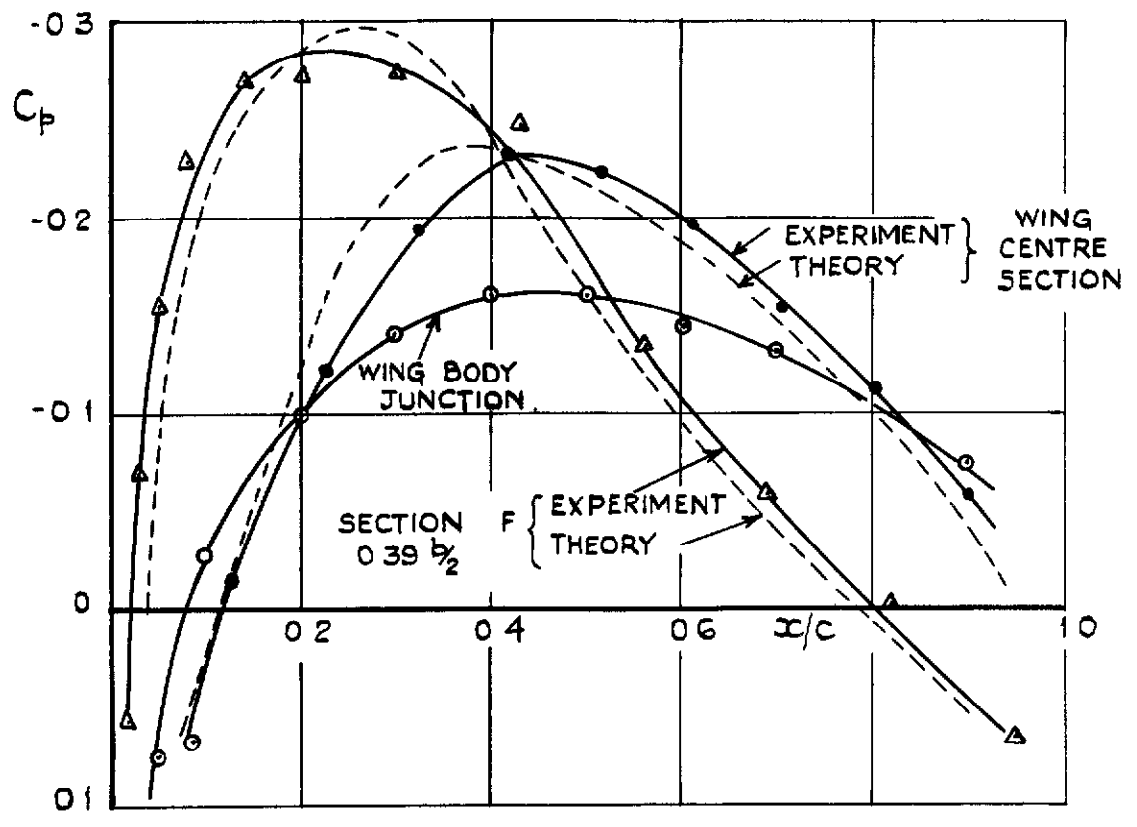

FIG. 4. COMPARISON OF PRESSURE DISTRIBUTIONS WITH THEORY, 59° WING, $\alpha = 0$, WITH & WITHOUT BODY.

FIG. 5.

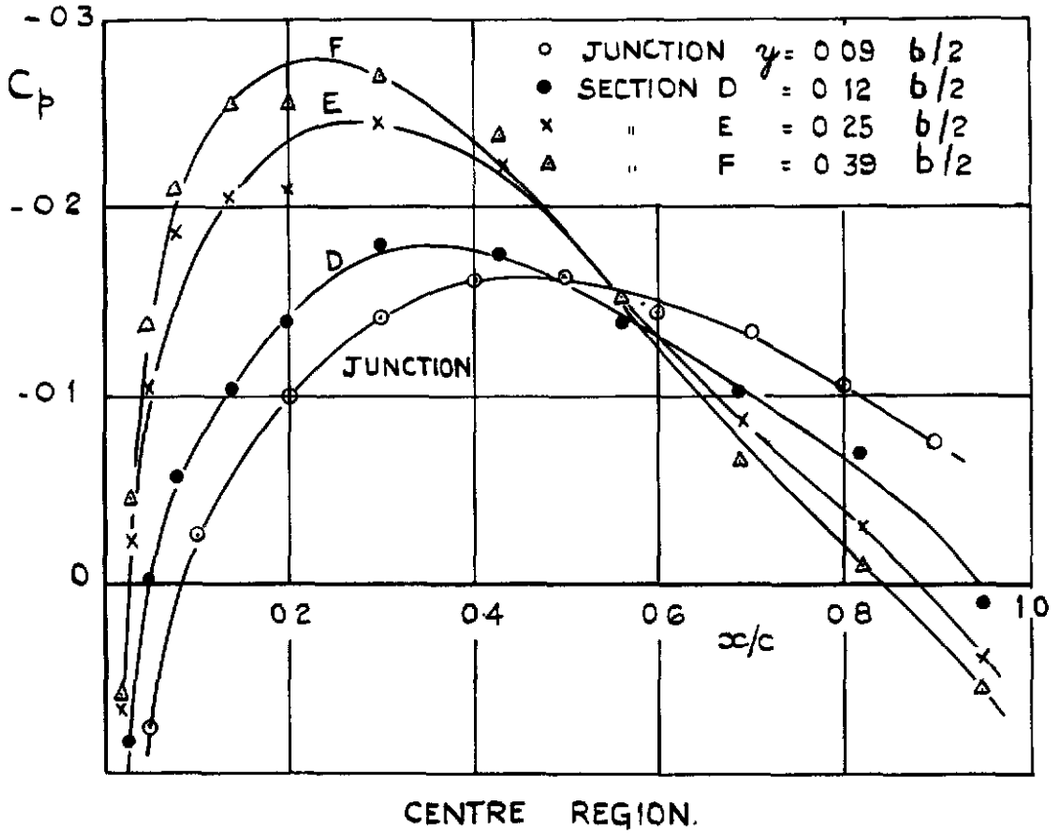

CENTRE REGION.

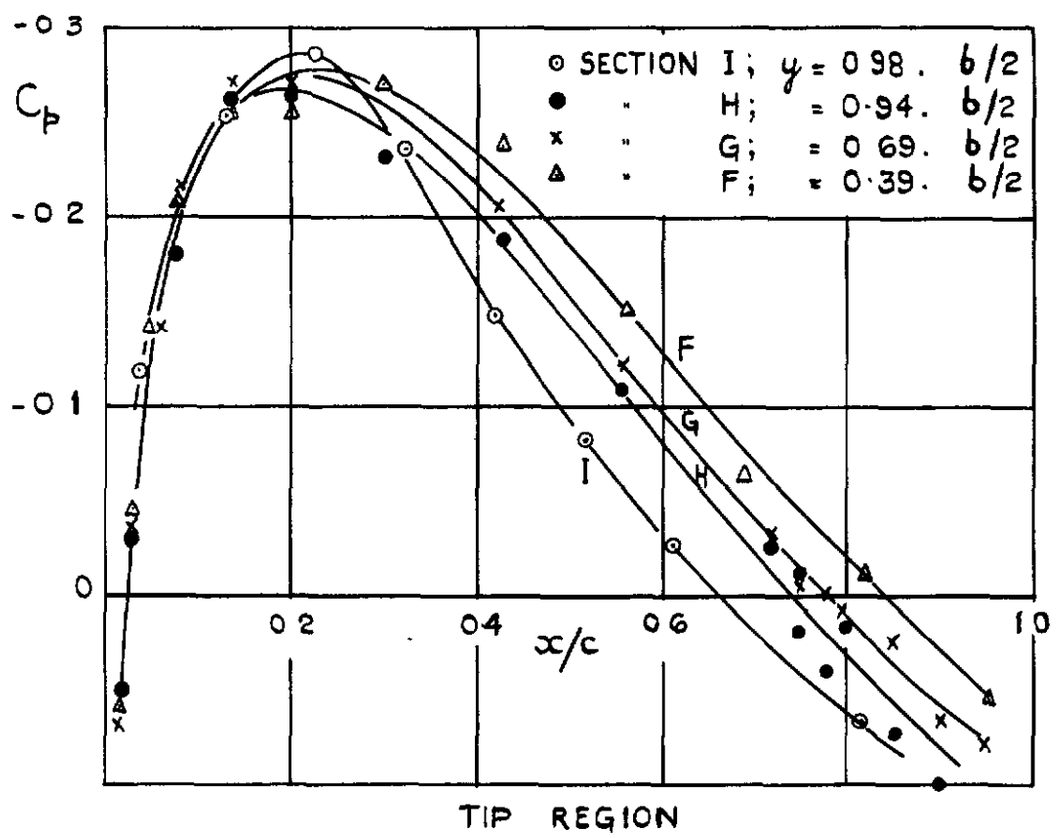

TIP REGION

FIG. 5. PRESSURE DISTRIBUTION
59° WING, WITH BODY, $\alpha = 0$.

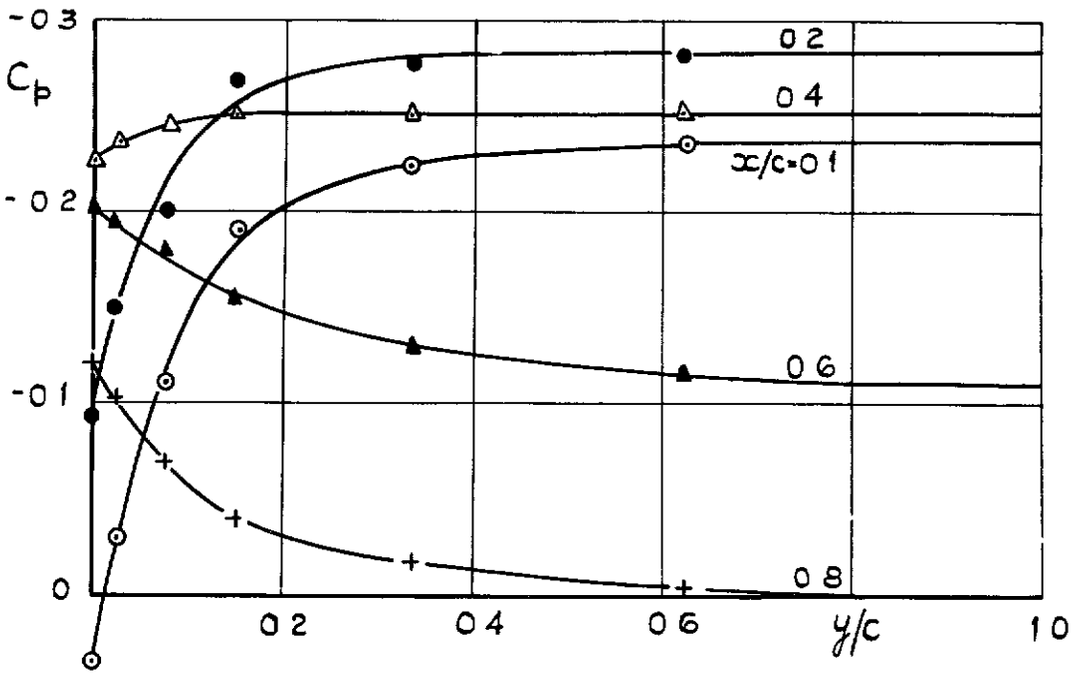

NO BODY.

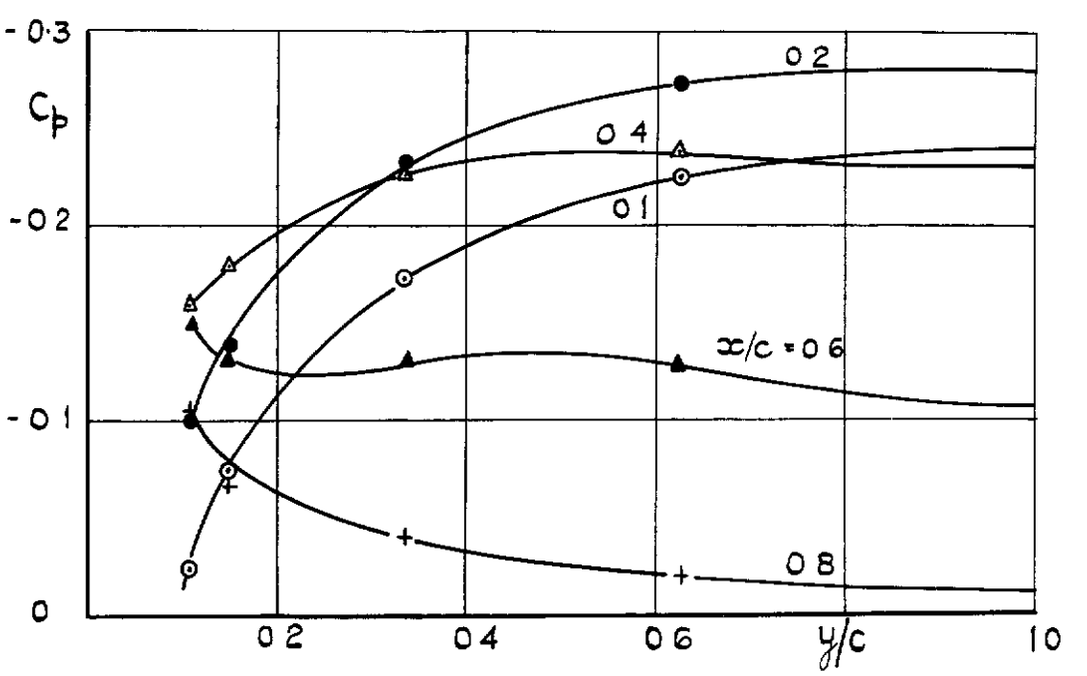

WITH BODY.

FIG.6 SPANWISE SPREAD OF EFFECT OF CENTRE SECTION, WITH AND WITHOUT BODY. 59° WING, $\alpha = 0$.

FIG. 7.

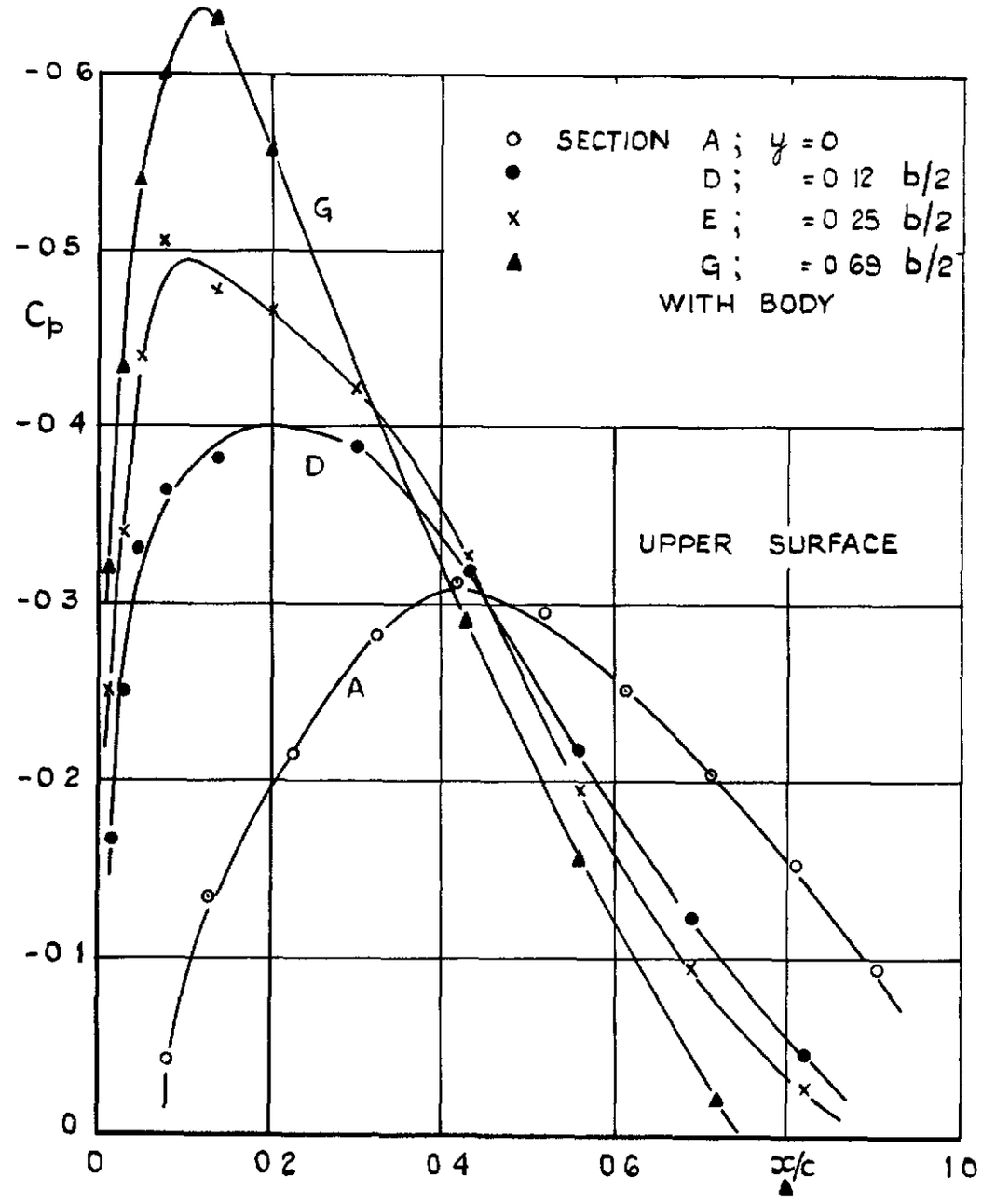

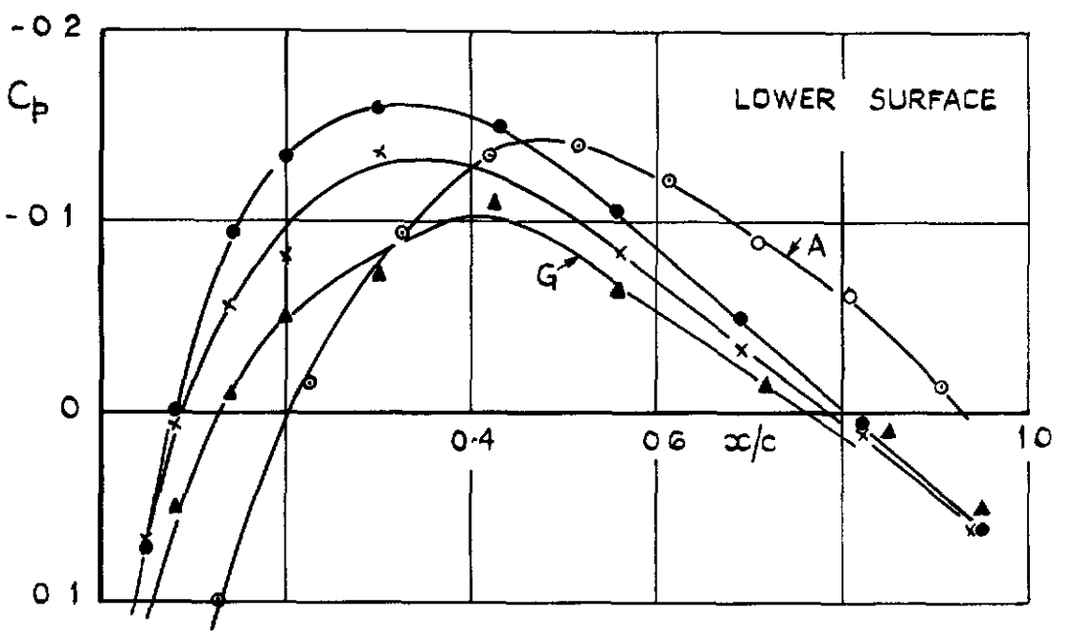

FIG. 7 PRESSURE DISTRIBUTION
59° WING, NO BODY, $\alpha = 4 \cdot 2°$

FIG. 8.

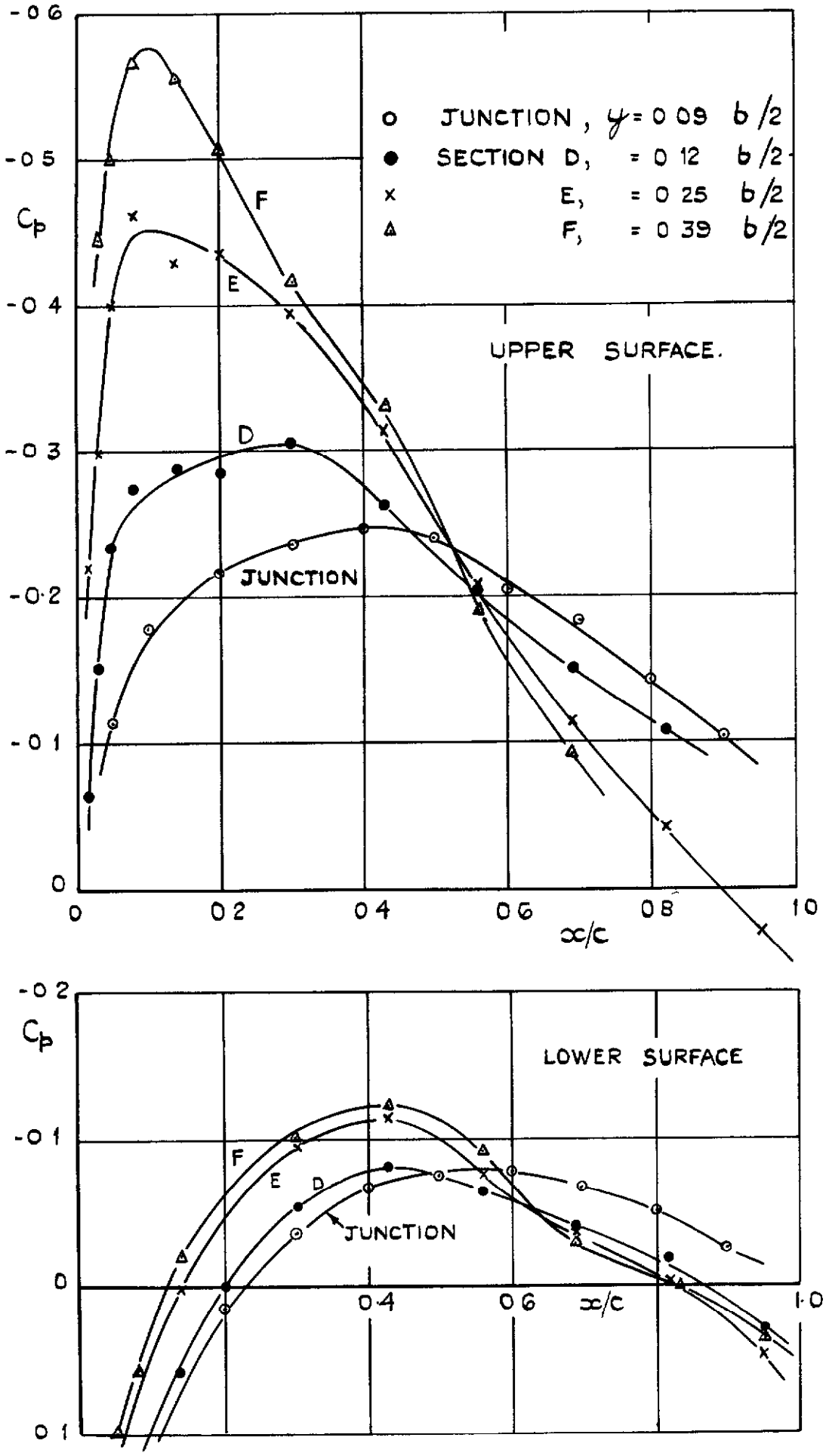

FIG. 8. PRESSURE DISTRIBUTION
59° WING, WITH BODY, $\alpha = 4 \cdot 2^\circ$

FIG. 9.

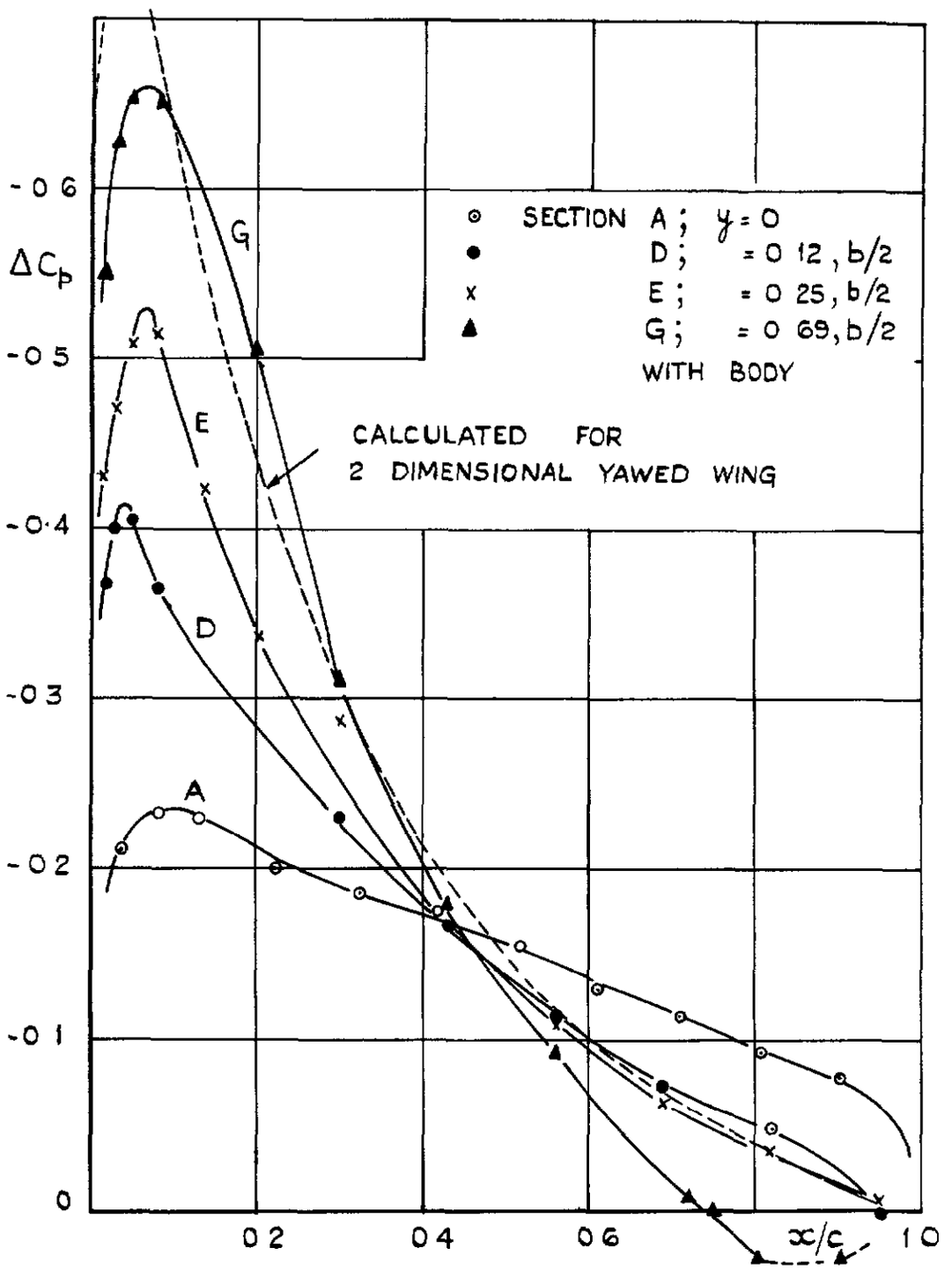

FIG. 9. CHORDWISE LIFT DISTRIBUTION.
59° WING, NO BODY, $\alpha = 4{\cdot}2^{\circ}$

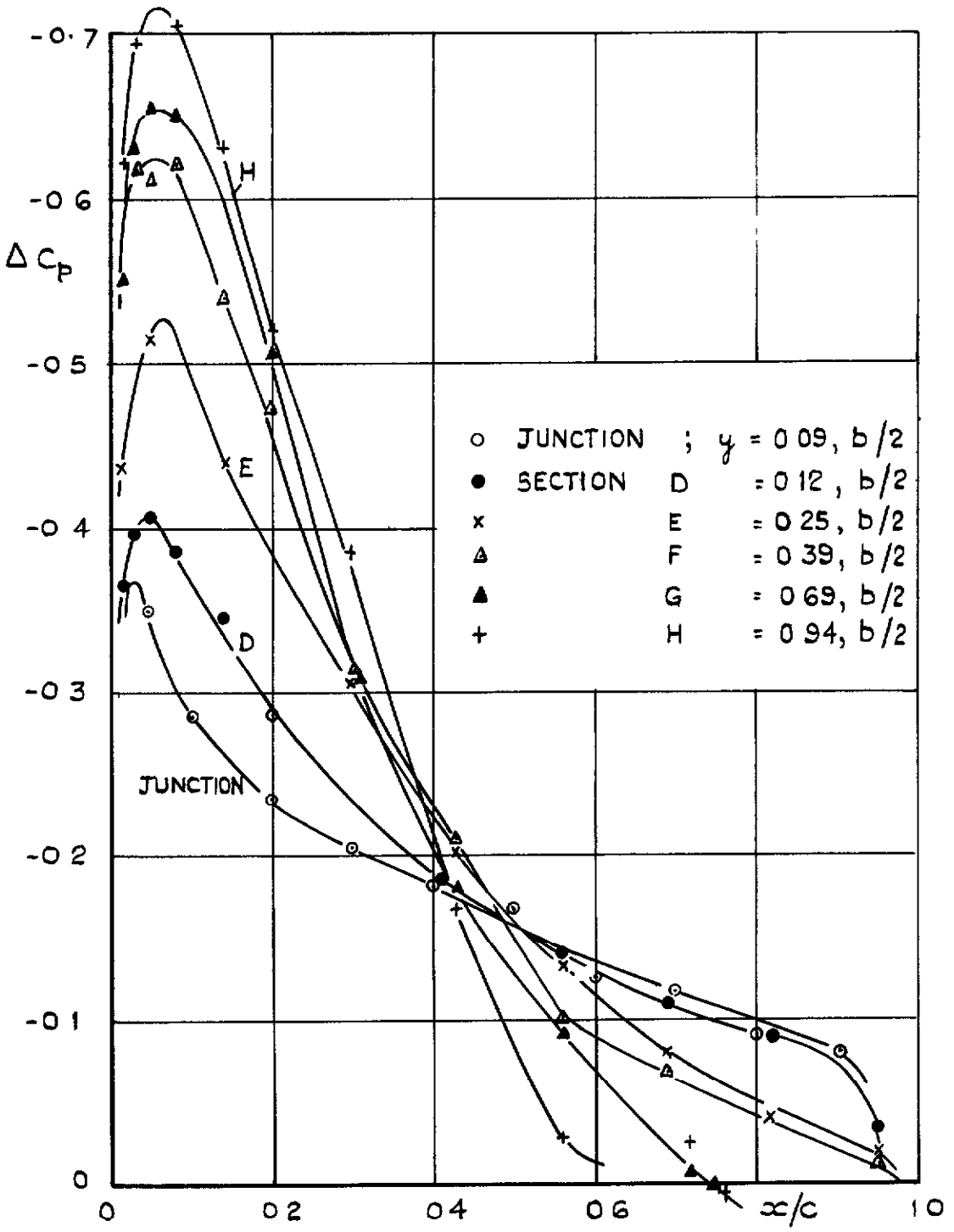

FIG. 10 CHORDWISE LIFT DISTRIBUTION 59° WING. WITH BODY, $\alpha = 4 \cdot 2^{\circ}$.

FIG. 11.

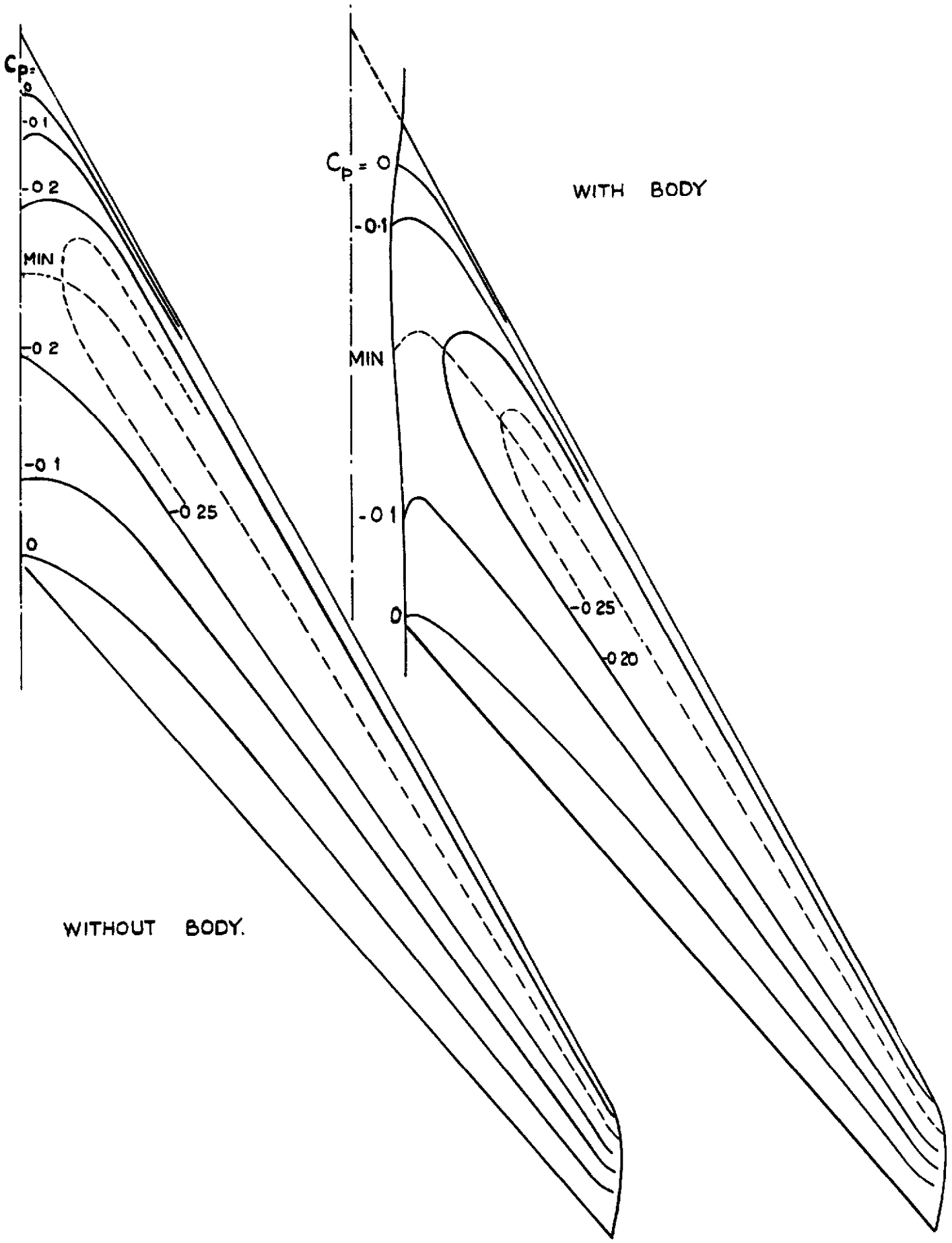

FIG. 11. ISOBARS ON 59° SWEPT WING
$\alpha = 0°$

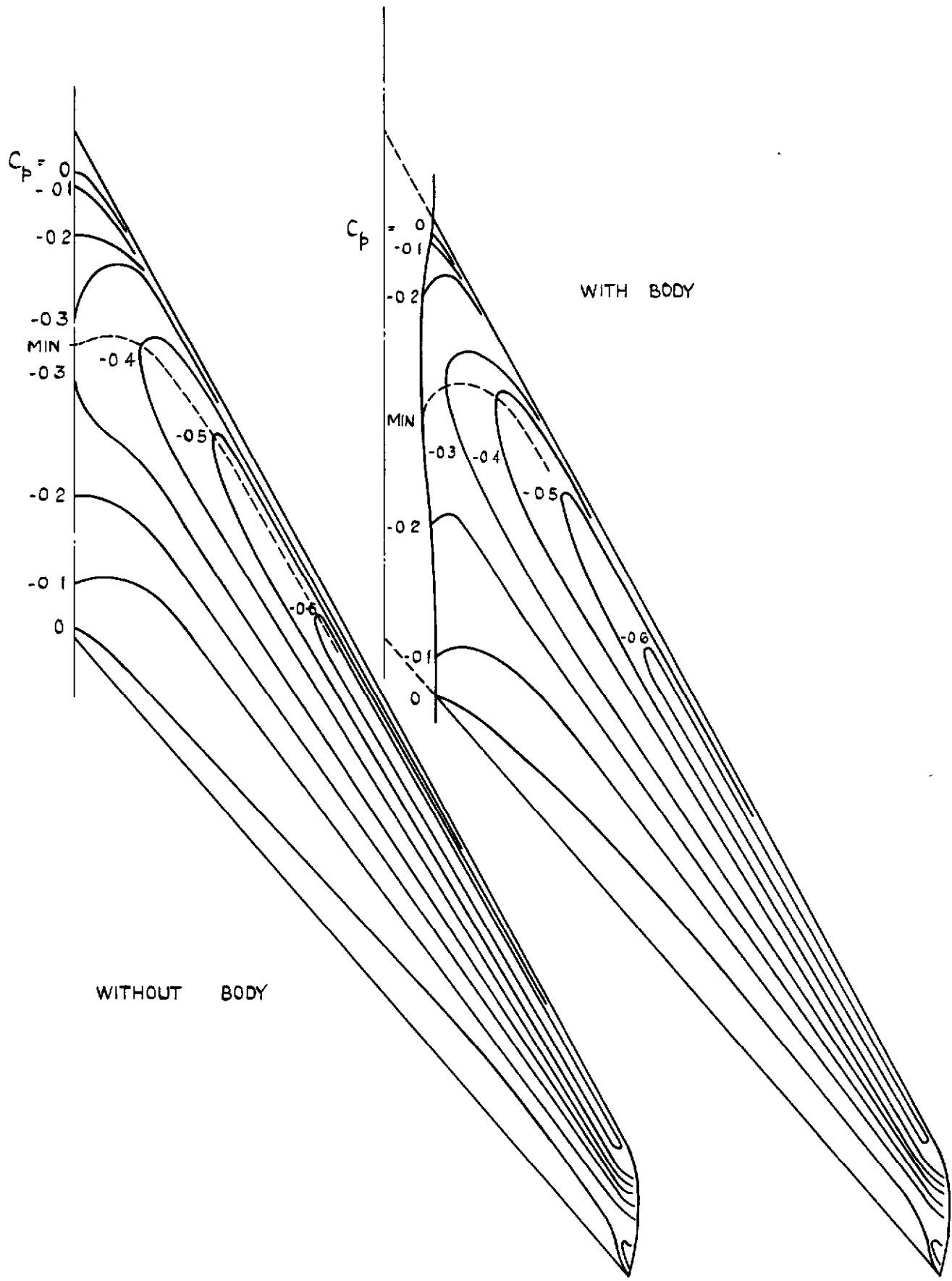

FIG. 12. ISOBARS ON 59° SWEPT WING.

$\alpha = 4 \cdot 2°$

FIG 13.

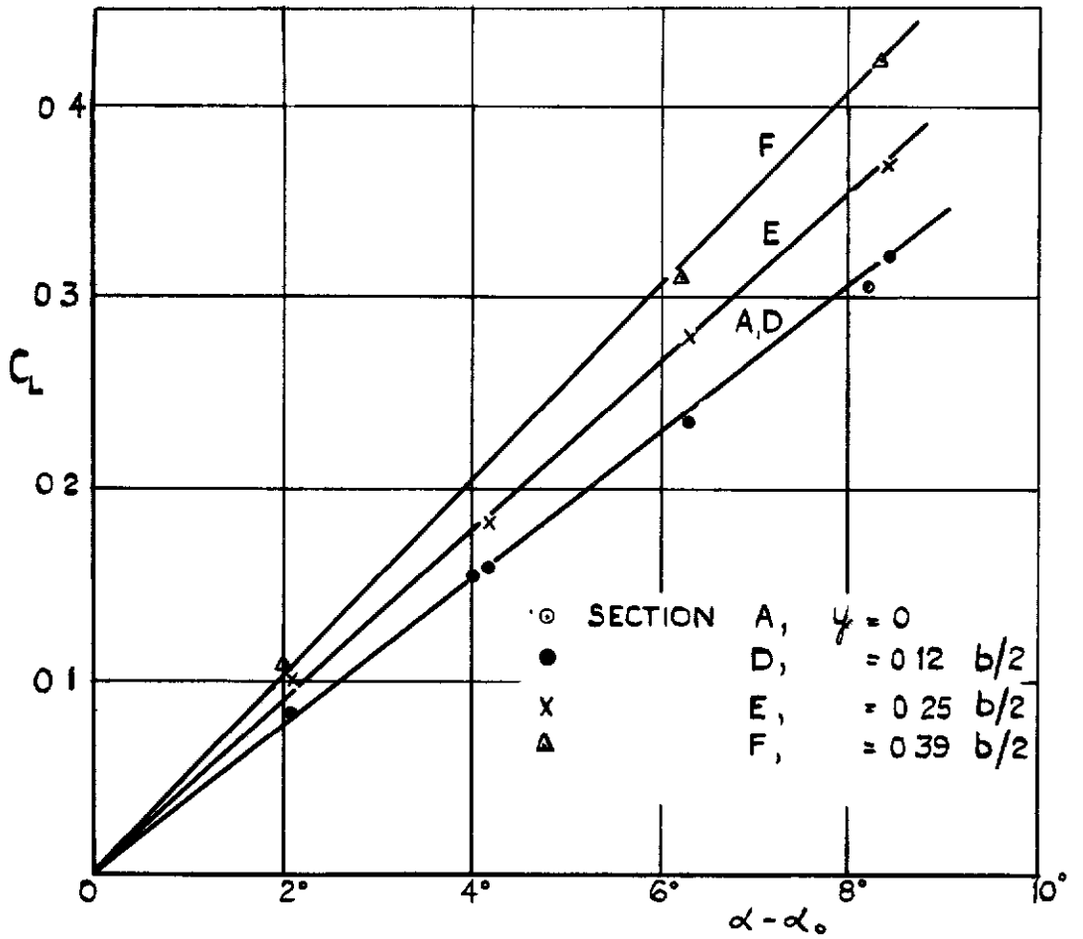

WITHOUT BODY.

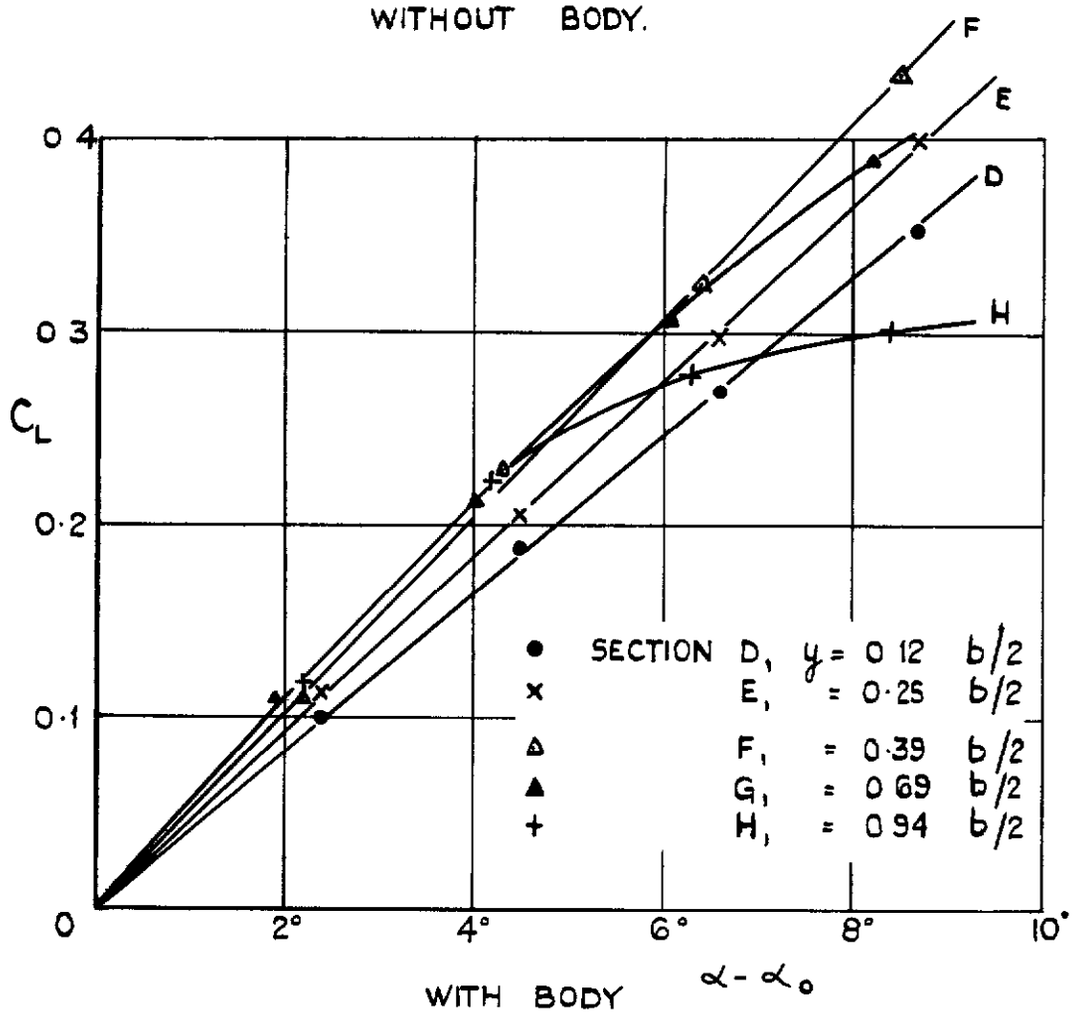

WITH BODY

FIG.13. LOCAL LIFT COEFFICIENTS.

FROM PRESSURE MEASUREMENTS.

59° WING.

FIG. 14.

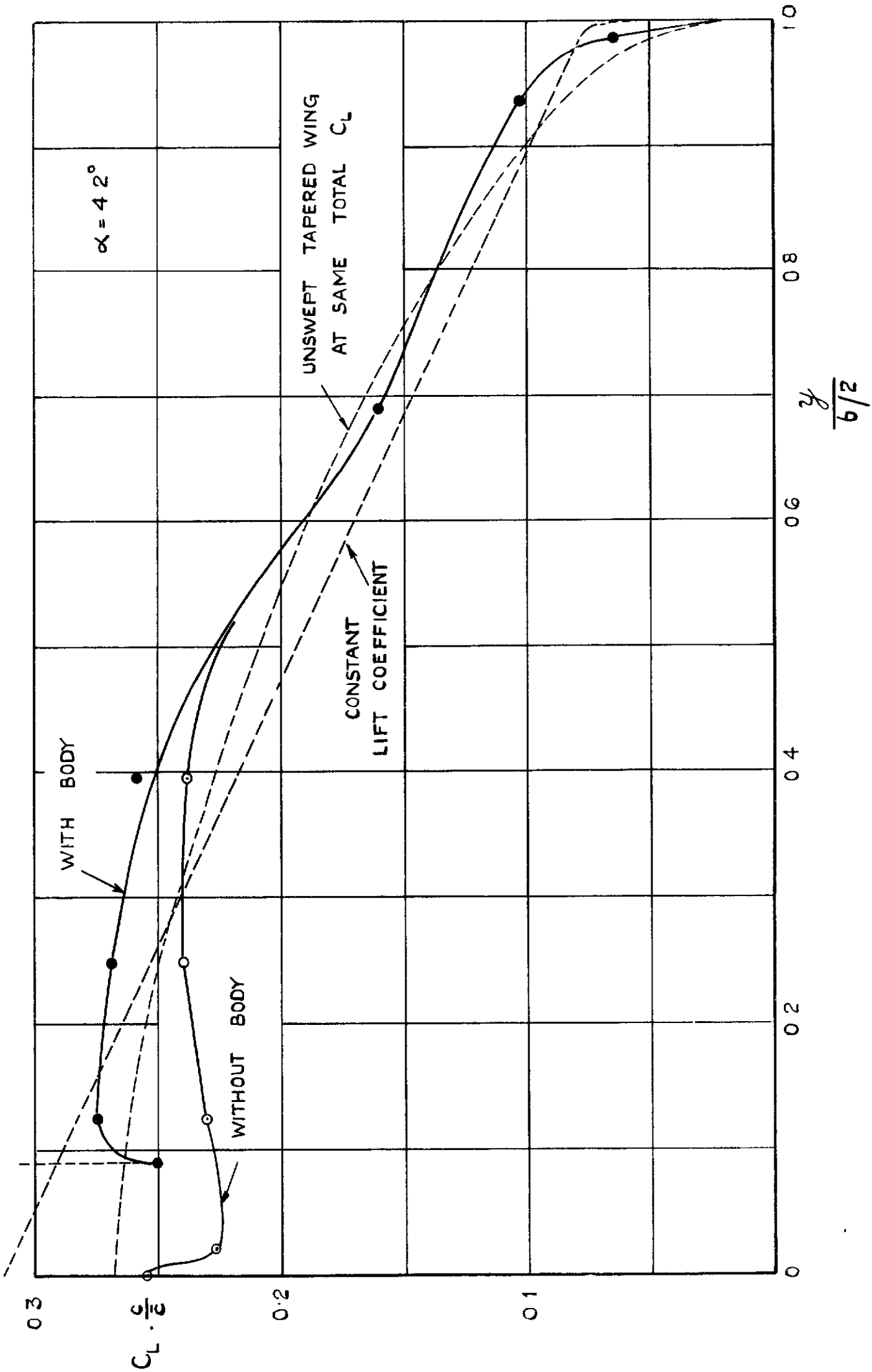

FIG. 14. SPANWISE LIFT LOADING OF 59° SWEPT WING. COMPARED WITH UNSWEPT WING.

FIG. 15 & 16.

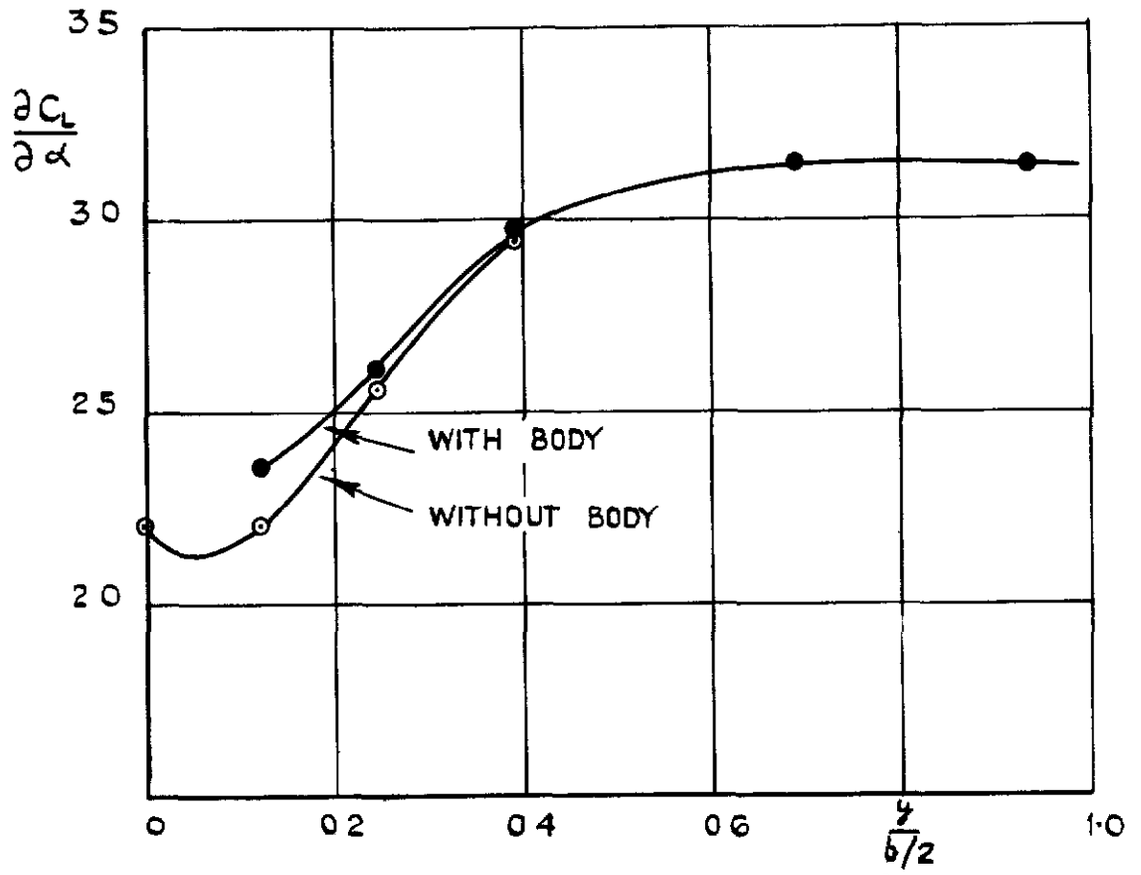

FIG. 15. LOCAL LIFT SLOPE ON 59° SWEPT WING
BALANCE MEASUREMENT
GIVES 2·65 (WITH BODY)

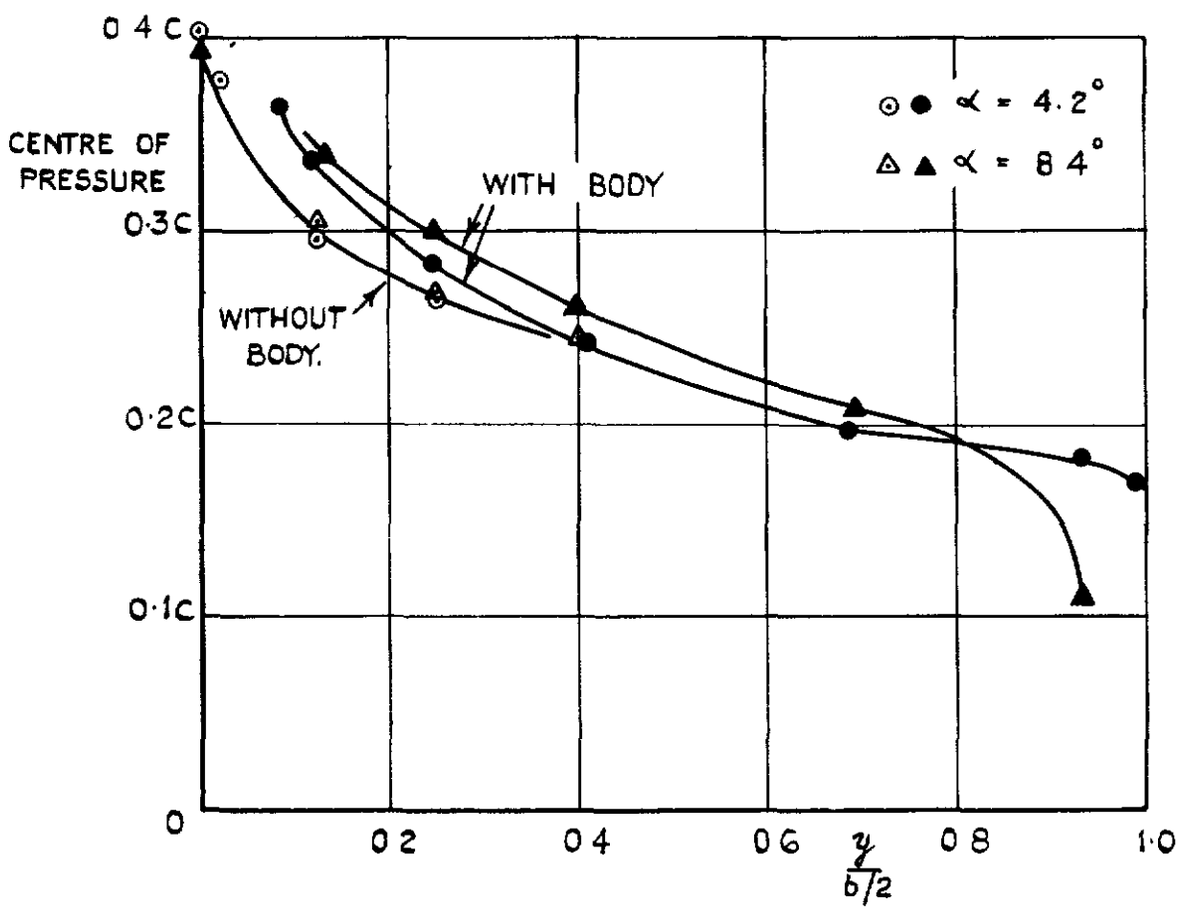

FIG. 16. LOCAL CENTRE OF PRESSURES.
59° WING.

FIG.17.

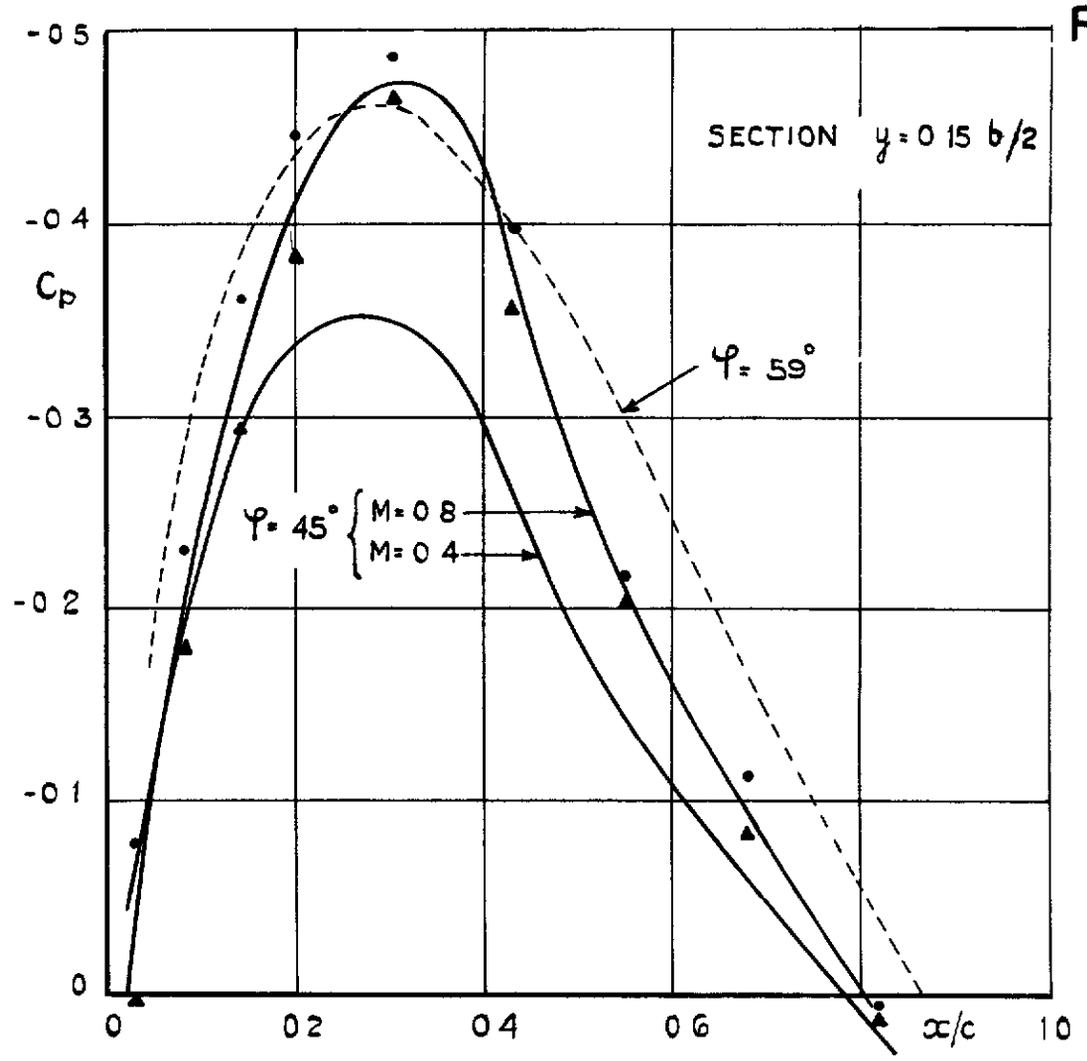

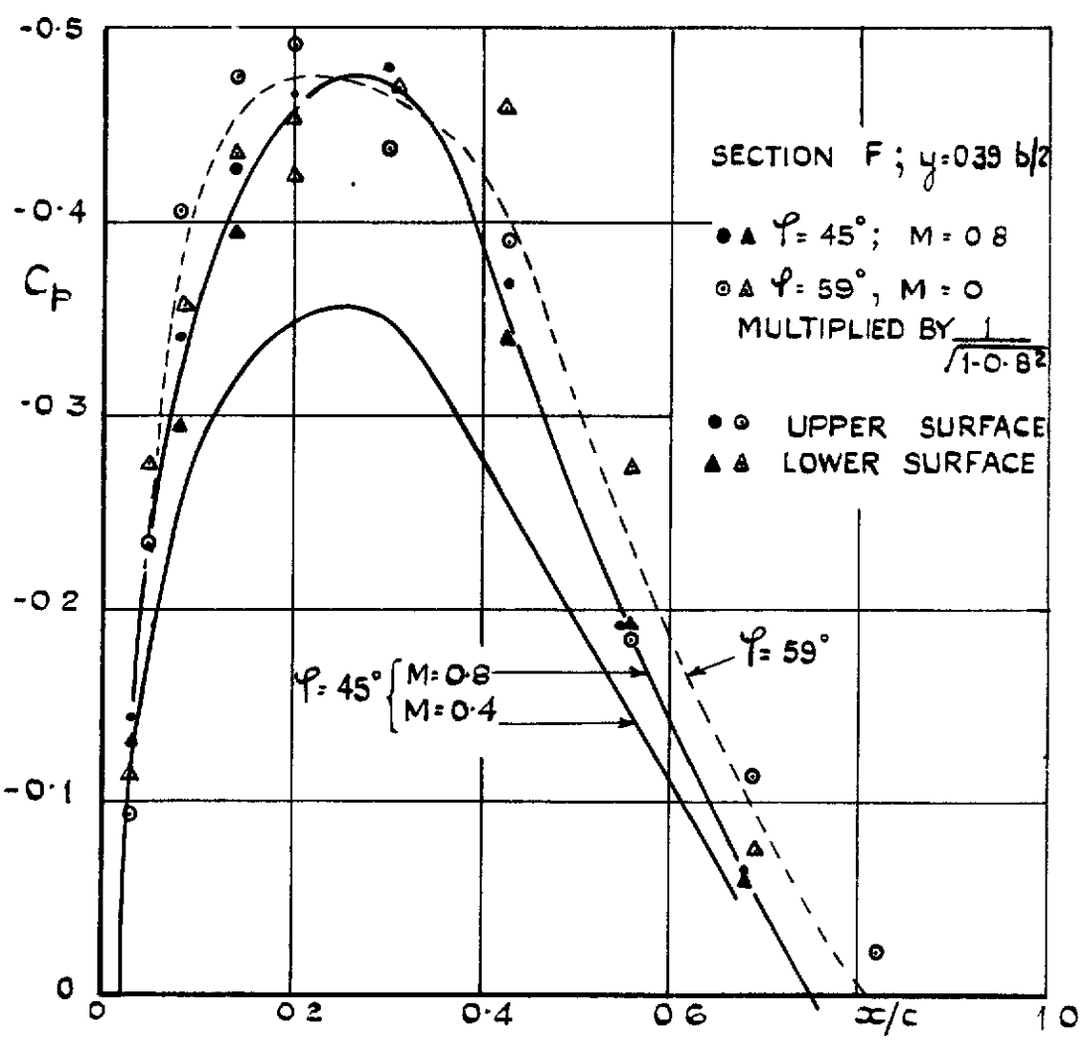

FIG.17. COMPARISON OF LOW SPEED AND HIGH SPEED MODELS, PRESSURE DISTRIBUTIONS. NO BODY, $\alpha = 0$.

FIG.18

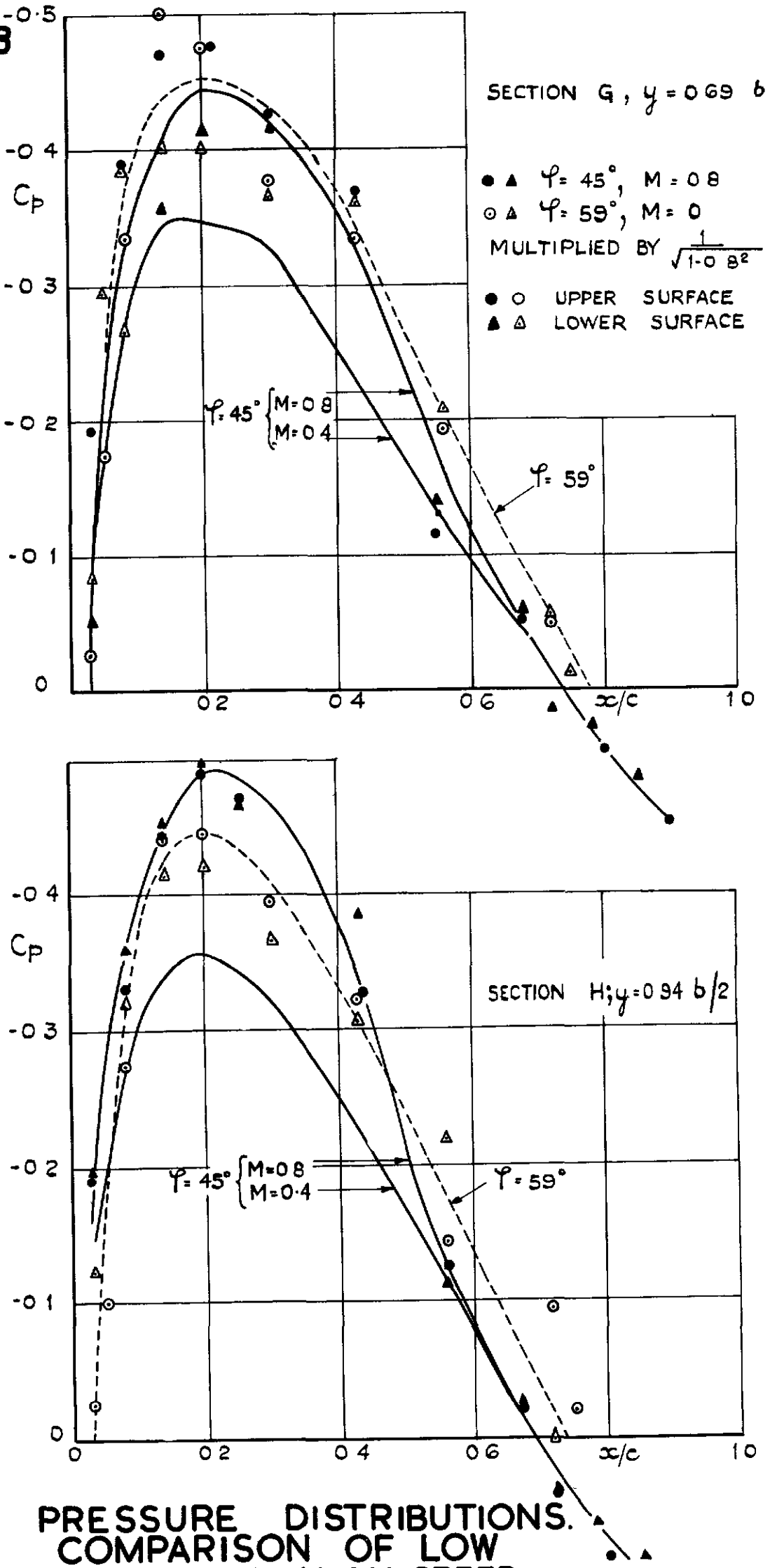

FIG.18 PRESSURE DISTRIBUTIONS. COMPARISON OF LOW SPEED AND HIGH SPEED MODELS, NO BODY, $\alpha = 0$.

FIG. 19.

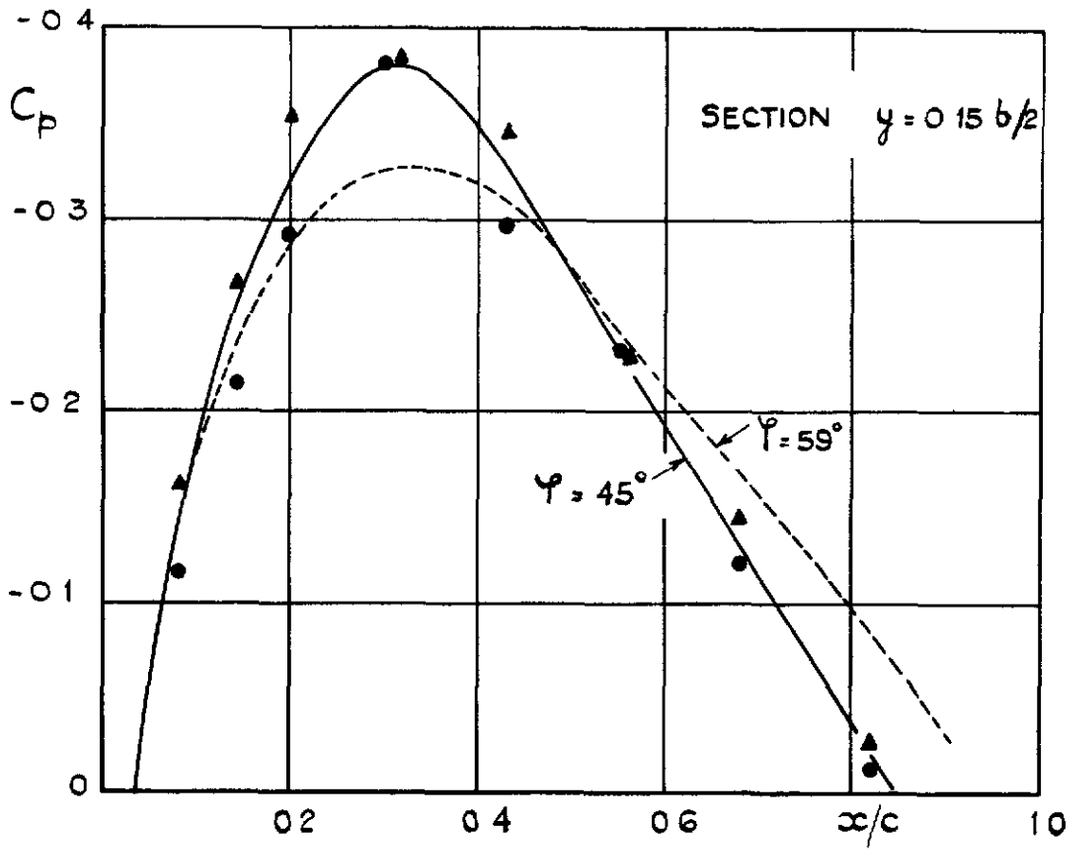

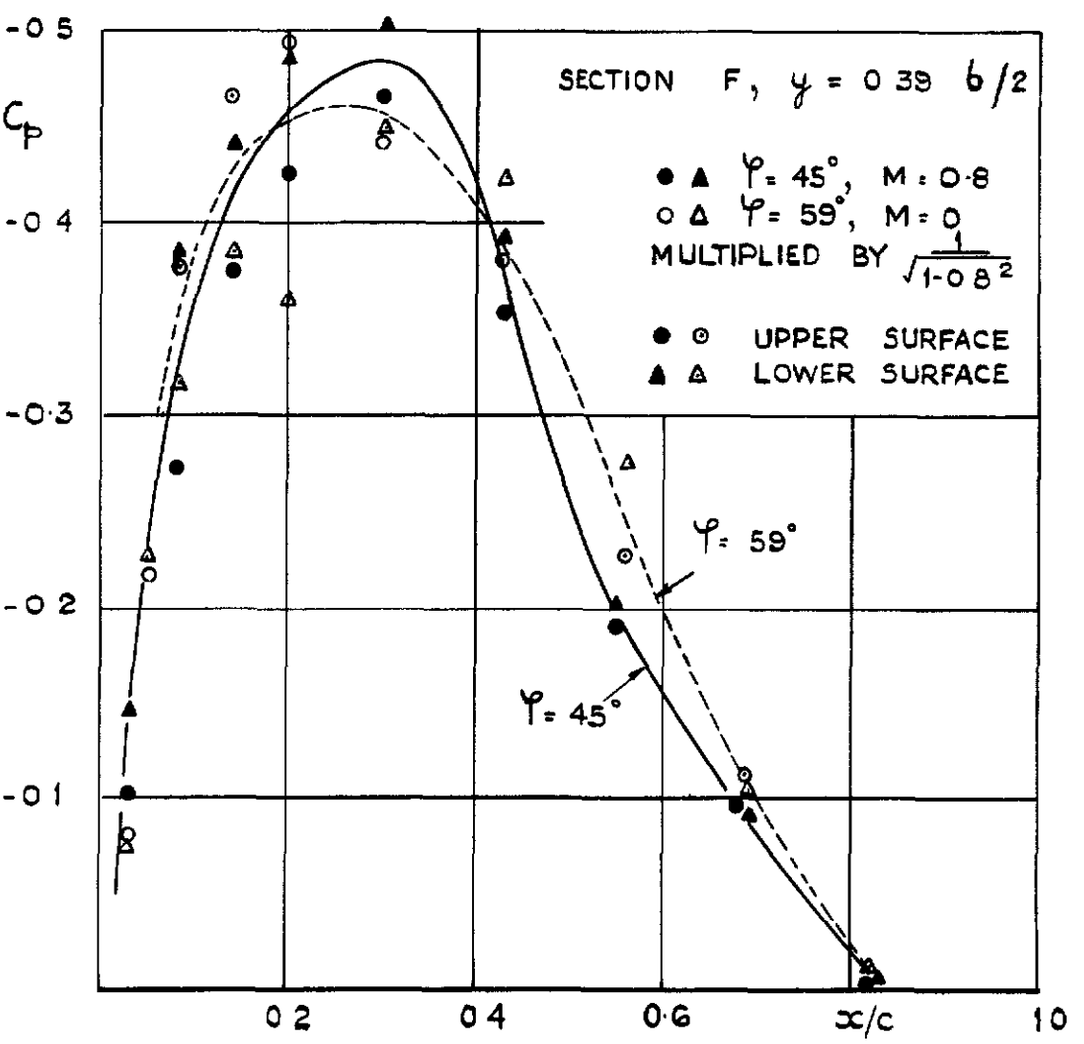

FIG. 19. COMPARISON OF LOW SPEED AND HIGH SPEED MODELS, PRESSURE DISTRIBUTIONS, WITH BODY, $\alpha = 0°$.

FIG. 20.

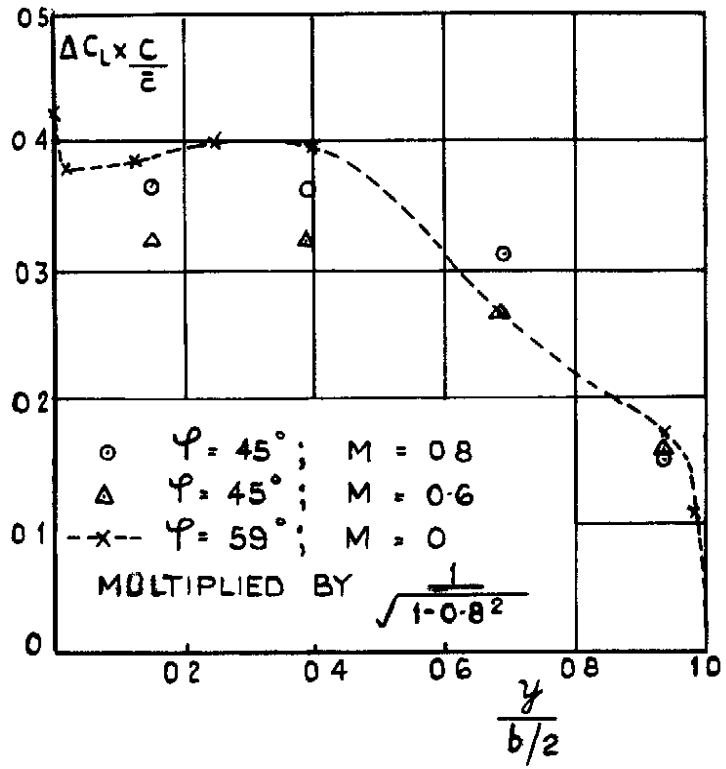

LIFT LOADING

$\Delta C_L = (C_L)_{\alpha=4°} - (C_L)_{\alpha=0°}$

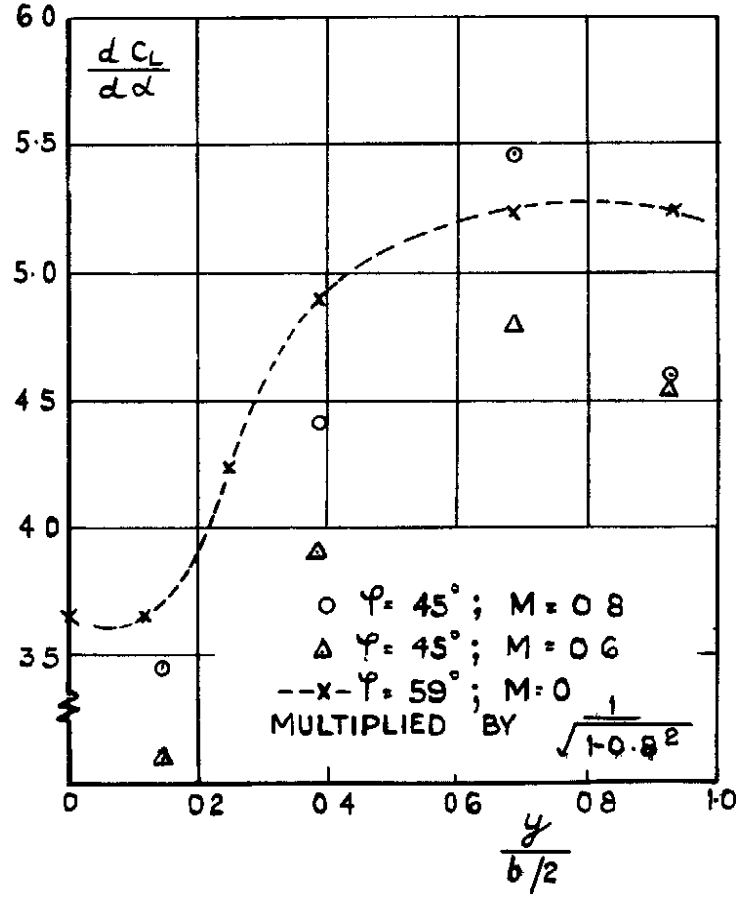

LOCAL LIFT SLOPE

$\alpha = 0°$

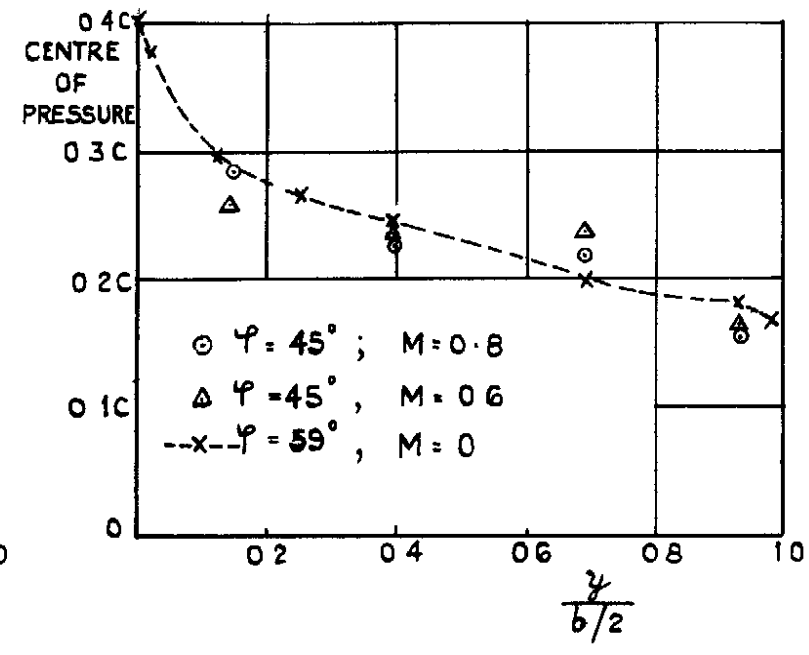

CENTRE OF PRESSURE

$\alpha = 0°$

FIG. 20. COMPARISON OF HIGH SPEED WING (45°) AND LOW SPEED WING (59°), NO BODY

FIG. 21.

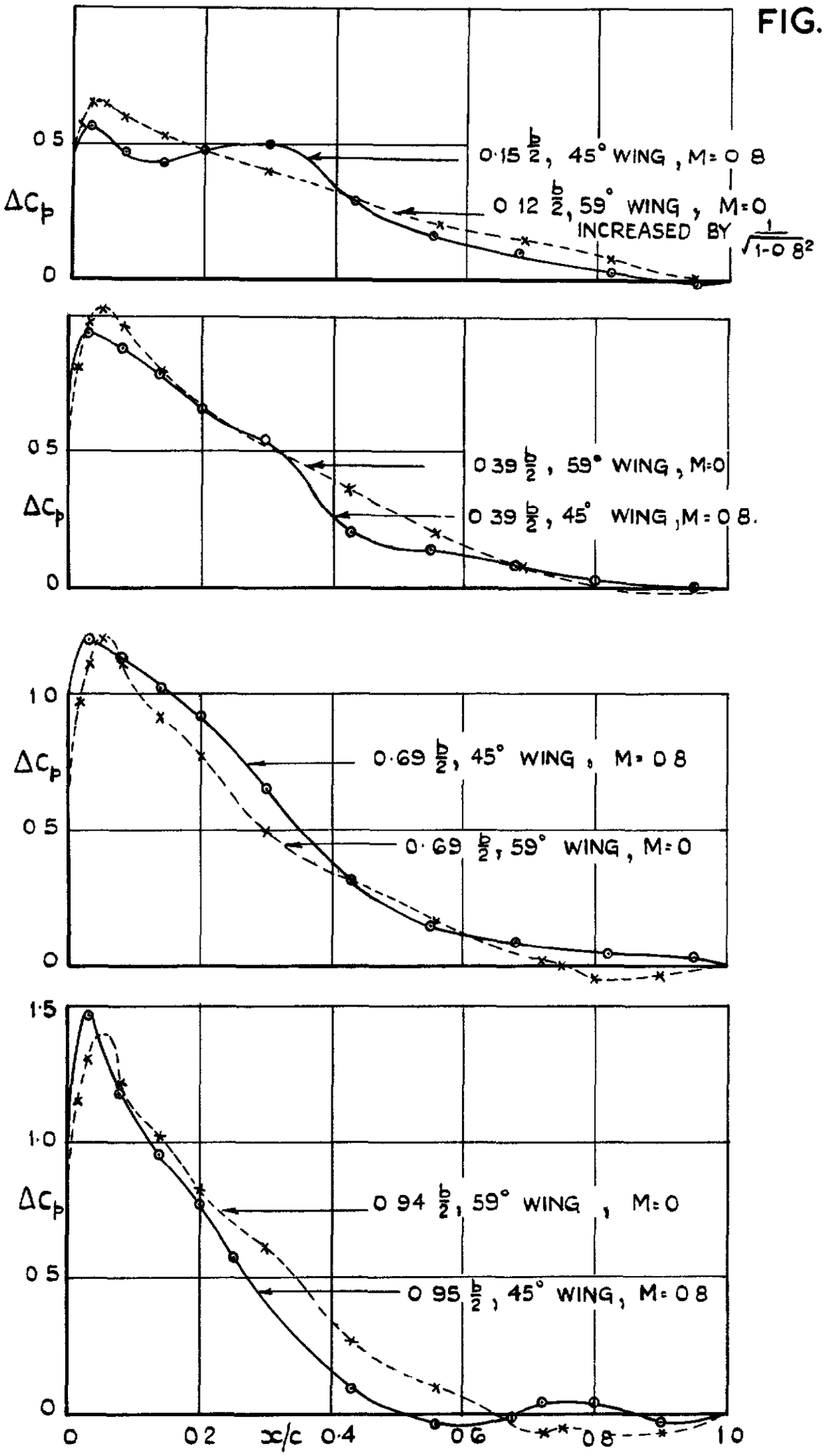

$$\Delta C_p = \left\{ C_p \text{ UPPER SURFACE} \quad C_p \text{ LOWER SURFACE} \right\}_{\alpha = 4.2^\circ} - \left\{ C_{p_U} - C_{p_L} \right\}_{\alpha = 0^\circ}$$

FIG. 21. COMPARISON OF CHORDWISE LOADINGS 45° & 59° WINGS.

Report No. Aero.2311a

August, 1950.

(Continuation of Aero Report 2311)

Part II

by

G.G.Brebner, M.A.

SUMMARY

Measurements have been made of the boundary layer at the trailing edge of a 59° sweptback wing at low speed. The total head, velocity and angle of flow have been found throughout the region in which these quantities differ from their free stream values. A new type of yawmeter was used.

The displacement thickness and its associated loss of lift are considerable: they rise quickly with incidence and vary along the span. Thus the spanwise loading will be quite different from that calculated on the basis of potential flow, even at comparatively small incidences.

LIST OF CONTENTS

LIST OF APPENDICES

LIST OF ILLUSTRATIONS

1 Introduction

A 59° sweptback wing, aspect ratio 3.6, taper ratio 4:1, was tested in the No.2 11½ ft × 8½ ft wind tunnel at the R.A.E. for comparison purposes with analogous model tests in the High Speed Tunnel. The results of pressure plotting tests (Ref.1) showed differences in the spanwise lift loading compared with calculations, for instance those by the Falkner method (Ref.2). The present note describes further tests carried out on the same wing to try to determine how much of the difference is due to boundary layer effects. The boundary layer flow was examined at 0.01c behind the trailing edge, at spanwise stations F ($\frac{y}{b/2} = 0.25$) and G ($\frac{y}{b/2} = 0.69$); the angle between this flow and the free stream direction, and the change in total head in the boundary layer were both measured.

2 Details of Model and Method

2.1 Details of Model

The model tested was the low-speed model of Ref.1 and details of the model are contained therein. The model was tested with the body in position.

2.2 Apparatus and Method

For the examination of the wake, a new type of yawmeter was used, designed by O.Conrad of Göttingen; nothing has so far been published about this instrument. It is illustrated in Fig.1. The yawmeter head consists of two 1 mm diameter tubes soldered together and filed to a point. The non-dimensional pressure difference in the two tubes is proportional to ϑ, the angle of yaw between the yawmeter and the flow, for a range $-10° \leq \vartheta \leq +10°$.

A calibration was also made with the yawmeter at an angle of pitch of 6°: this showed no difference from the run at zero pitch. The trailing edge angle of the wing section is 14°, so it is assumed that this instrument will read satisfactorily the flow following the upper and lower surface of this trailing edge at ±7° pitch.

Fig.2 shows the calibration curve obtained for the Conrad yawmeter compared with that obtained for a conventional type of yawmeter, showing the increased sensitivity. The pressures in the two tubes approximate more closely to the values at a point than do those read on a conventional type of yawmeter. Moreover, a pointed instrument such as this is almost unaffected by changes of Reynold's Number.

The Conrad yawmeter was mounted on a metal bracket, which could be fixed to the wing surface in a position clear of the section being examined. The screwed rod, R, (Fig.1) could be adjusted to be vertical at zero incidence, and the mounting was arranged so that the yawmeter rotated about the vertical axis through the apex A, which consequently remained fixed during rotation. The yawmeter could be rotated from outside the tunnel by a cord over a pulley while a run was in progress, and a scale engraved on the lower pulley P enabled the amount of rotation to be read after the run.

The above arrangement permits an extension of the use of the yawmeter beyond the usual one of measuring the pressure difference in

two tubes and reading the angle of flow from a calibration curve. In the present tests, the yawmeter was set at the positions on each side of the flow direction for which the pressure difference was a predetermined value, about 0.1q. The angle of flow was taken as the mean of these two settings, and related to the direction of free stream flow, which was assumed to have been reached at about 2" vertically from the trailing edge, i.e. at 0.06 and 0.1 z/c at sections E and G respectively. From these pressures and angles the dynamic pressure and total head at that point may be obtained in terms of their free stream values. The method of calculating these is given in the Appendix, which also describes a simpler variation of this use of the yawmeter.

3 Tests

The tests were made in the No.2 $11\frac{1}{2}$ ft × $8\frac{1}{2}$ ft wind tunnel at the R.A.E. during October 1949. The wake immediately behind the trailing edge was examined at two spanwise sections, E (y = 0.25 b/2) and G (y = 0.69 b/2) of Ref.1, the yawmeter being mounted so that it was about 0.2" behind the trailing edge (i.e. 0.01 and 0.005 times local chord at G and E respectively). Velocity, dynamic pressure, total head and angle of flow were found throughout that part of the wake in which they differed from the free stream values, for $\alpha = -0.6^\circ$, 1.5°, 3.6° and 5.7° at section G and for $\alpha = -0.6^\circ$ and 3.6° at section E. The wind speed was 120 f.p.s. The Reynolds number was 1.23×10^6 at section G and 2.10×10^6 at section E, corresponding to local chord values of 19.5" and 33.4".

4 Results and Discussion

The total head, velocity, and angle of flow measurements are plotted against z/c in Figs.3 and 4. These show that, as the incidence increases, the wake thickness increases on the upper surface and decreases or the lower surface, the overall thickness increasing for $\alpha = 3.6^\circ$ and over at section G, but showing little increase at 3.6° on section E, which is nearer the centre of the wing. It is worthy of note that, for $\alpha = 3.6^\circ$ and 5.7°, the velocity and total head do not decrease all the way down to the trailing edge, but have an approximately constant value over a z/c range depending on the incidence. Moreover the maximum angle between the local flow and the free stream direction increases with incidence. At $\alpha = 5.7^\circ$ it is about 40° and approximately constant from z/c = 0.005 to z/c = 0.02. Since the angle of sweep at the trailing edge is 49°, these facts suggest that, next to the wing surface at the trailing edge, there is a layer of air flowing almost parallel to the trailing edge, in which the total head and velocity are almost constant.

Fig.3 shows a comparison between the flow at sections E and G for $\alpha = 3.6^\circ$: this shows that the vertical extent of the wake in terms of the local chord, and the thickness of the constant velocity layer, both increase towards the tip, while at zero incidence there is little difference in the extent of the wake.

The effect of boundary layer on lift for straight wings has already been studied by several authors, the most recent report being by Preston (Ref.3). The loss of lift due to boundary layer is associated with the displacement thickness of the layer, δ^*, defined as $\int_0^\delta \left(1 - \frac{V}{V_1}\right) dz$, where V is the velocity in the boundary layer at distance z from the surface and V_1 is the velocity at distance δ,

the edge of the boundary layer. Fig.5 shows the displacement thickness on the upper surface at the trailing edge plotted against positive and negative angles of incidence at sections E and C. In this case the displacement thickness calculated was $\delta_x^* = \int_0^\delta \left(1 - \frac{V_x}{V_{1x}}\right) dz$, where V_x and V_{1x} are the x-components of V and V_1 (x measured along the undisturbed wind direction). Since the wing profile is symmetrical, Fig.5 indicates that the displacement thickness is greater on the upper surface than on the lower surface, and that it increases with incidence more rapidly at section C than at section E. This is due to the effect shown in Fig.3, the region of low velocity outflow near the surface increasing in thickness towards the wing tip. This increase of δ_x^* with increase of α and y is characteristic of swept wings because of the presence and variation of the outflow. The loss of lift, being associated with the displacement thickness, will vary in a similar manner to δ_x^*.

The decrease of lift is evident in Fig.6 where the measured values of C_L against α (curves (a)) are compared with curves (c) calculated by the method of reference 4 for a 14% thick profile in potential flow without boundary layer, and after making allowance for the profile thickness. The tangent to (a) at $\alpha = 0^\circ$, curve (b), does not coincide with (c). The difference between (b) and (c) indicates that δ_x^* and the associated lift loss include a term proportional to α, and the difference between (a) and (b) indicates that they include a term proportional to α^2. This latter term is mainly due to sweep, as can be seen from Fig.5 where it is much greater at section C than at section E.

Since δ_x^* and the loss of lift are different at different spanwise positions, the whole spanwise distribution is altered, and Fig.7 shows that this alteration is appreciable at the comparatively small incidence of 6.3°.*

Further work on this kind of boundary layer investigation on swept-back wings is being done, and will be published shortly.

References

No.	Author	Title, etc.
1	Tunnel Staff of Aero. Dept.	Low Speed Pressure Distributions on a 50° Swept Wing. A.R.C. 12,377. (Part I of this Report)
2	V.M. Falkner	A Comparison of Two Methods of Calculating Wing Loading with Allowance for Compressibility. R & M. 2685 October, 1949.
3	J.H. Preston	The Calculation of Lift taking account of the Boundary Layer. R & M. 2725. November, 1949

---

* The experimental local lift coefficients plotted in Fig.7 are different from those given in Table XVII, Ref.1, having been calculated from the pressure distributions by a more accurate method.

References (Contd.)

No.	Author	Title, etc.
4	D. Kuchemann	A simple method for calculating the span and chordwise loadings on thin swept wings. A.R.C. 13,758. August, 1950.

Appendix

Determination of Static Pressure, Dynamic Pressure, Velocity and Total Head by the Conrad Yawmeter

Let p_1, p_2, be the pressures in the two tubes of the yawmeter,

p, q, H, V, be the static pressure, dynamic pressure, total head and velocity at the point being examined,

p_o, q_o, H_o, V_o, be the above quantities in the free stream,

ϑ be the angle between the yawmeter and the direction of local flow,

Θ be the angle between the local flow and the free stream flow.

The quantities measured on the sloping tube manometer are $\frac{p_1 - p_o}{q_o} = K_1$ and $\frac{p_2 - p_o}{q_o} = K_2$. In general, $p_1 = p + f_1(\vartheta) \cdot q$ and $p_2 = p - f_2(\vartheta) \cdot q$.

(a) Calibration of yawmeter

In the neighbourhood of the yawmeter, p, q and H are the same as p_o, q_o and H_o since no disturbing body is present. The calibration showed that

(i) $\frac{p_1 - p}{q} - \frac{p_2 - p}{q} = C_1 \cdot \vartheta$ within a range $-10^\circ \leq \vartheta \leq +10^\circ$

and (ii) $\frac{p_1 - p}{q} + \frac{p_2 - p}{q} = 2 \cdot C_2$, within a range $-10^\circ \leq \vartheta \leq +10^\circ$,

where C_1 and C_2 are constants determined by the calibration.

(b) Model Tests

In traversing the boundary layer the most convenient method is to rotate the yawmeter until $R_1 = R_2$, i.e. $\vartheta = 0^\circ$, and note $(R_1 + R_2)$ and the angle Θ from the free stream direction, which is assumed to be the flow direction at the measuring point furthest from the surface. Then turn the yawmeter through 10° and note R_1 and R_2. Assuming p_o, q_o and V_o to be known,

$$(R_1 - R_2)_{\vartheta = \pm 10^\circ} = \left(\frac{p_1 - p}{q} - \frac{p_2 - p}{q} \right) \cdot \frac{q}{q_o}$$

$$= 10 C_1 \cdot \frac{q}{q_o}, \text{ by (i).}$$

$$\therefore \frac{q}{q_o} = \frac{1}{1C\ C_1} (R_1 - R_2)_{\vartheta = \pm 10^o}$$

and $$\frac{V}{V_o} = \sqrt{\frac{q}{q_o}} .$$

Also

$$(R_1 + R_2)_{\vartheta = 0^o} = \left(\frac{p_1 - p}{q} + \frac{p_2 - p}{q} + 2 . \frac{p - p_o}{q} \right) \frac{q}{q_o}$$

$$= 2\ C_2 . \frac{q}{q_o} + 2 \frac{p - p_o}{q_o} , \text{ by (ii).}$$

$$\therefore \frac{p - p_o}{q_o} = \tfrac{1}{2} (R_1 + R_2)_{\vartheta = 0^o} - C_2 . \frac{q}{q_o}$$

$$\therefore \frac{p}{q_o} = \tfrac{1}{2} (R_1 + R_2)_{\vartheta = 0^o} - C_2 . \frac{q}{q_o} + \frac{p_o}{q_o}$$

and $$\frac{H - p_o}{H_o - p_o} = \frac{H - p}{H_o - p_o} + \frac{p - p_o}{H_o - p_o} = \frac{q}{q_o} + \frac{p - p_o}{q_o}$$

Hence, ignoring compressibility corrections, the velocity, static pressure, dynamic pressure and total head at points throughout the wake can be found in terms of their free stream values.

Wt.2078.CP86.53. Printed in Gre + Brit in.

FIG. I.

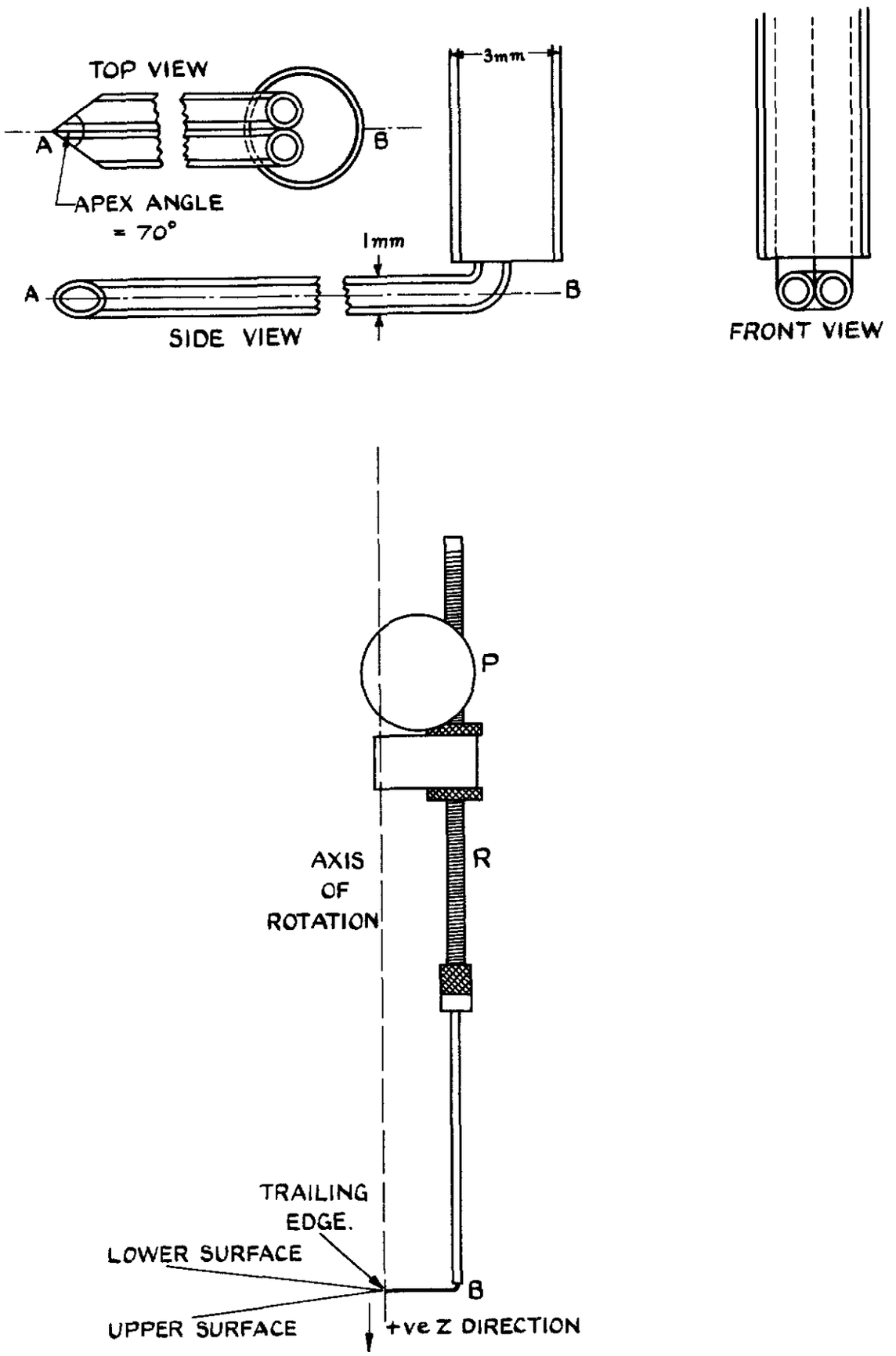

FIG. I. SKETCH OF CONRAD YAWMETER AND ITS INSTALLATION.

FIG. 2.

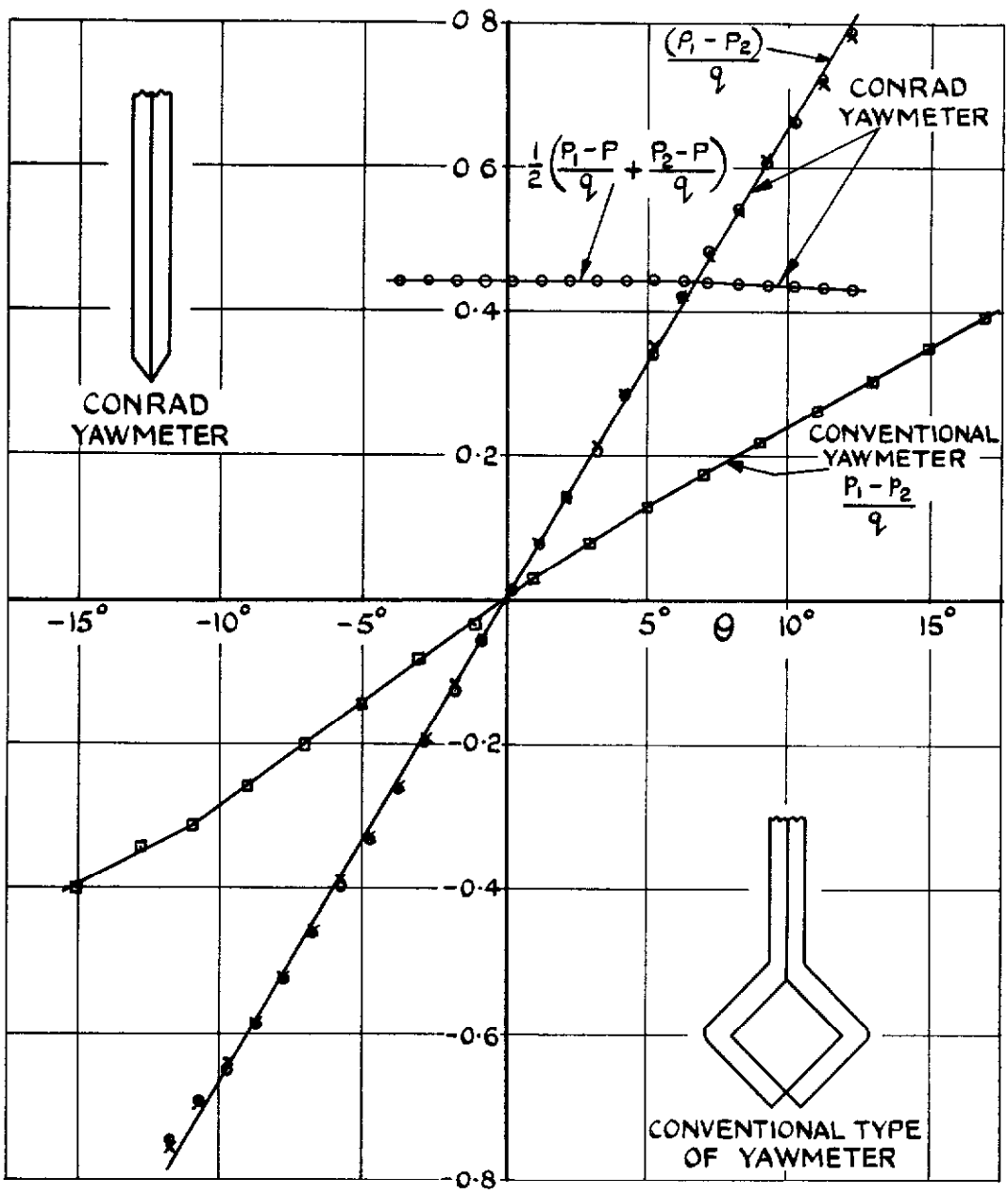

FIG. 2. CALIBRATION CURVES OF TWO DIFFERENT YAWMETERS

FIG. 3.

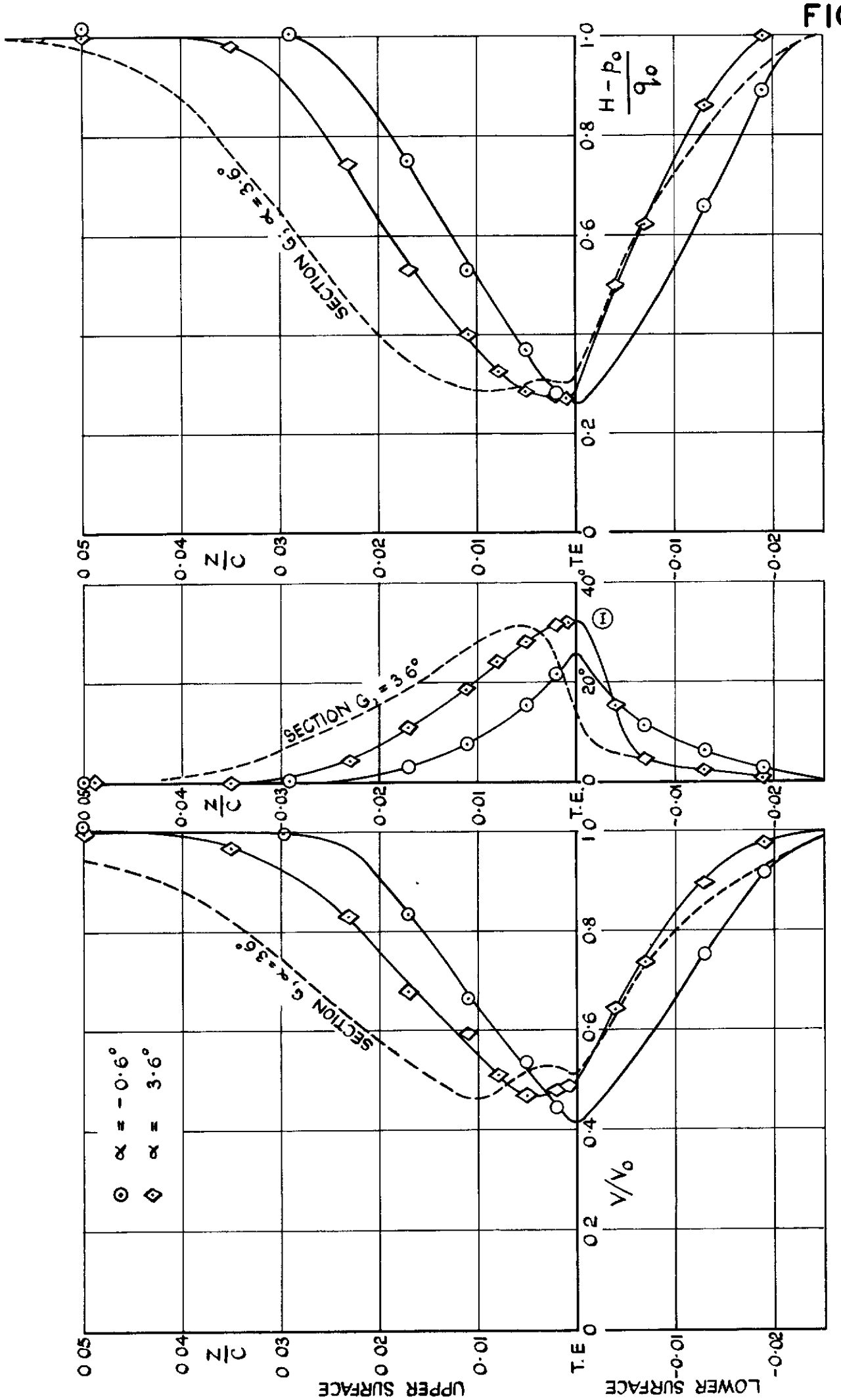

FIG. 3. VELOCITY, TOTAL HEAD AND ANGLE OF FLOW AT SECTION E. $y = 0 \cdot 25\, b/2$

FIG. 4.

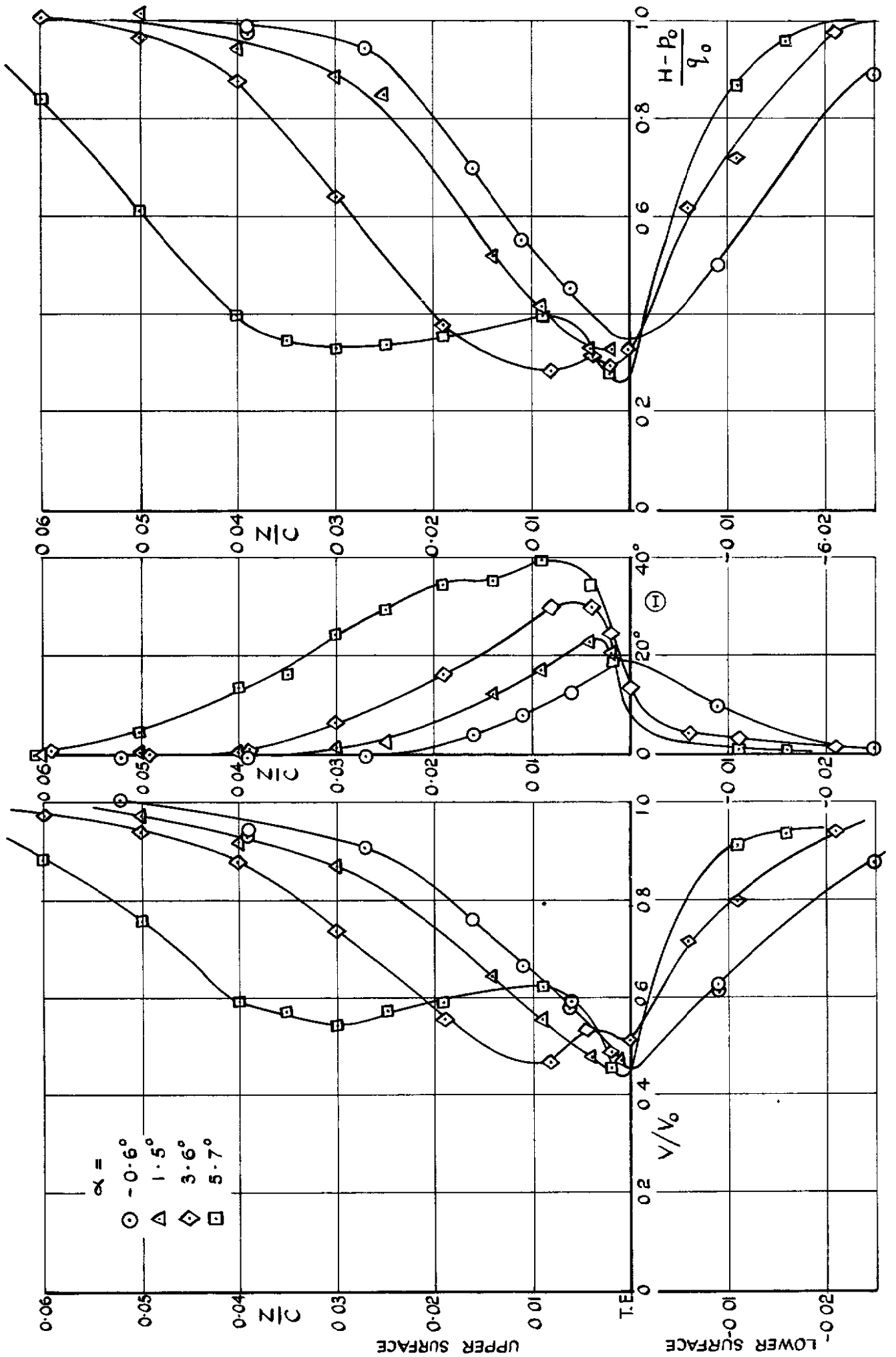

FIG. 4. VELOCITY, TOTAL HEAD AND ANGLE OF FLOW AT SECTION G, $y = 0{\cdot}69\ b/2$

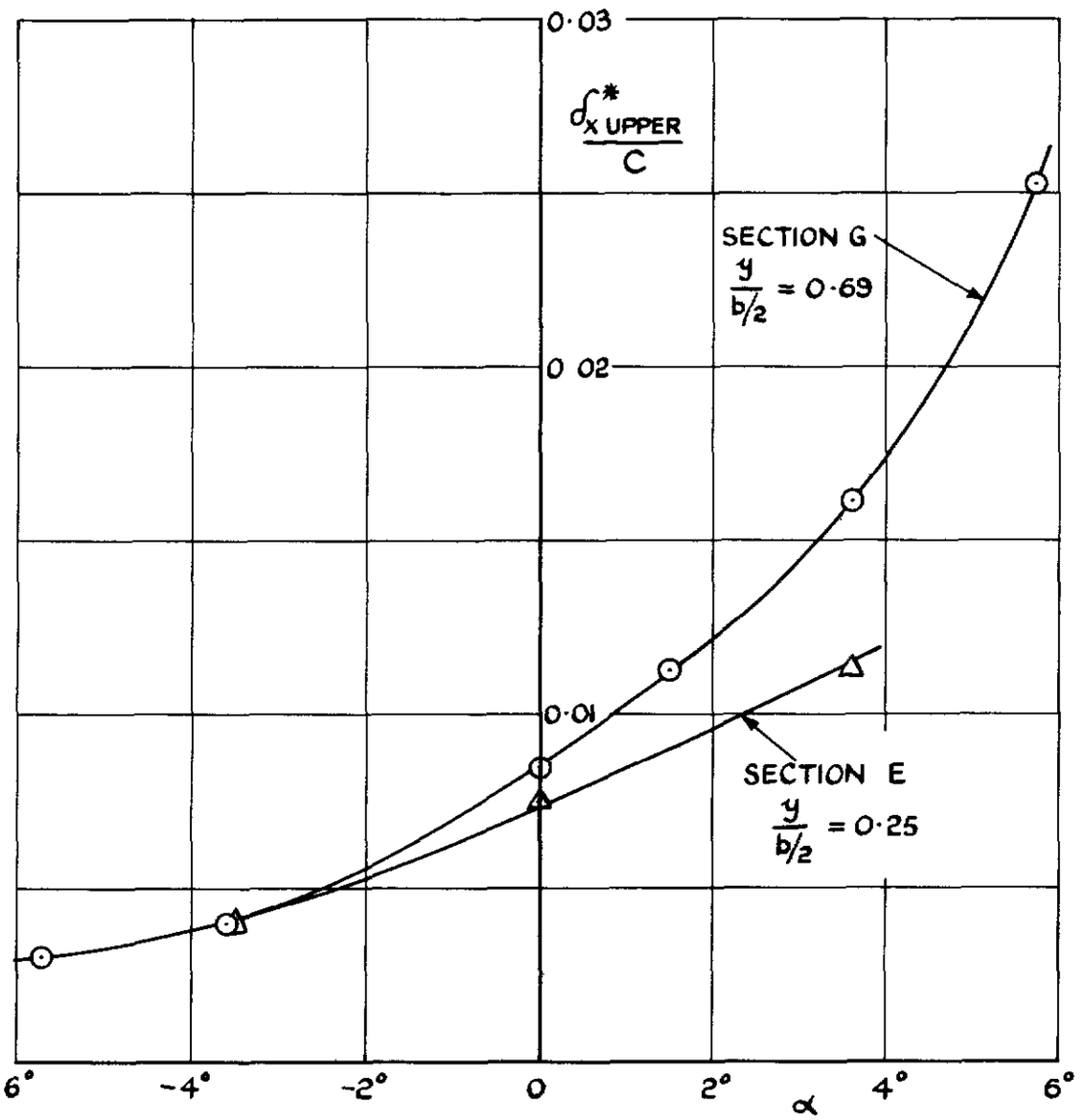

FIG. 5. DISPLACEMENT THICKNESSES ON UPPER SURFACE AT THE TRAILING EDGE AT TWO SPANWISE POSITIONS.

FIG. 6 & 7.

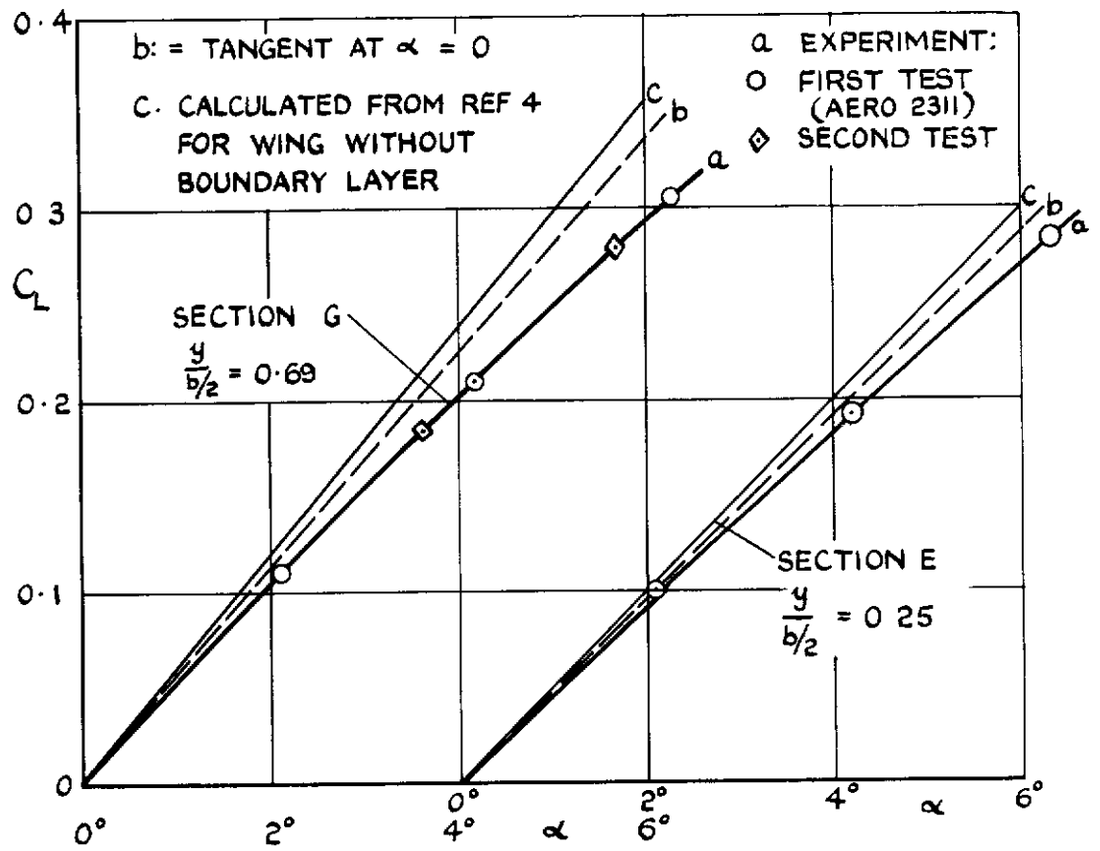

FIG. 6. LOCAL LIFT COEFFICIENTS AT SECTIONS E&G.

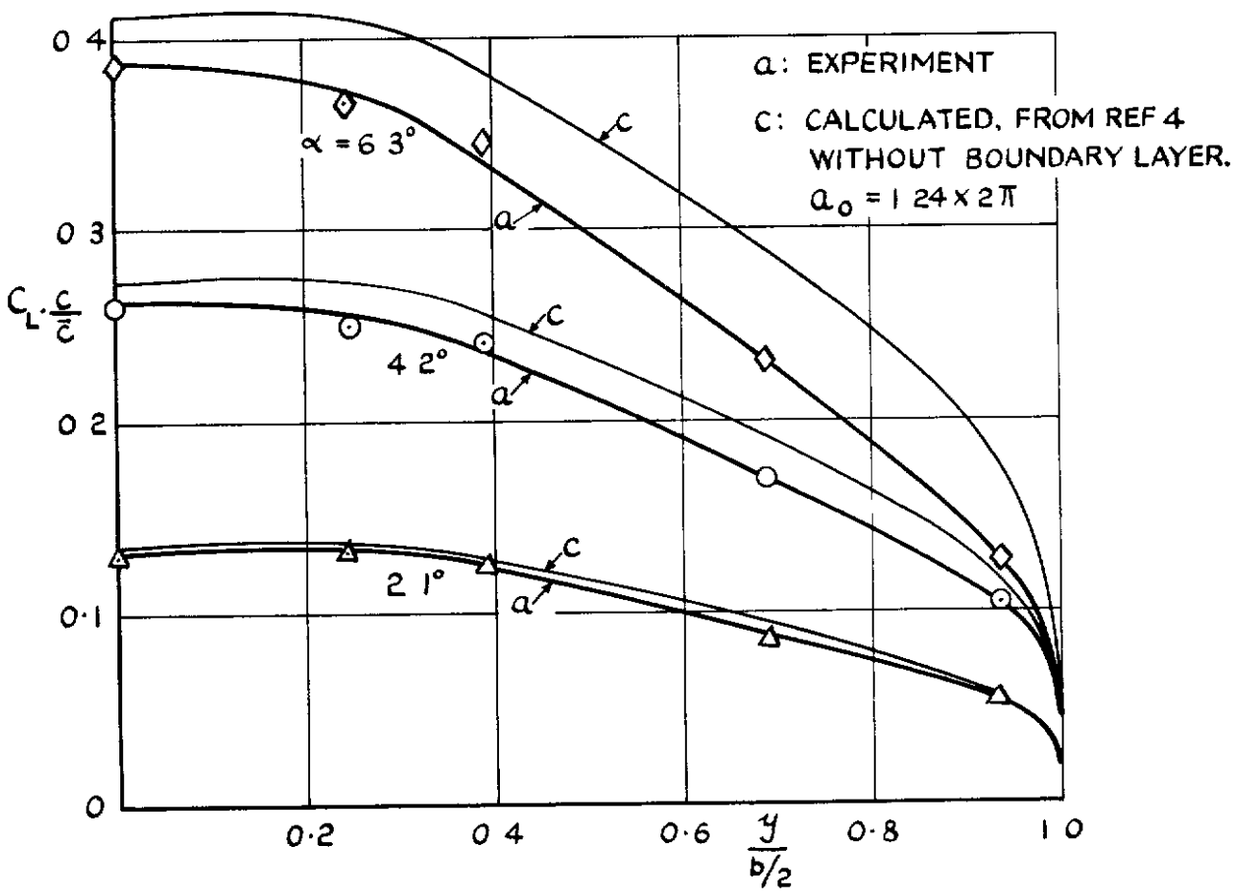

FIG. 7. SPANWISE LIFT DISTRIBUTIONS AT THREE INCIDENCES.

C.P. No. 86
(12,377, 13,735)
A.R.C. Technical Report

PUBLISHED BY HER MAJESTY'S STATIONERY OFFICE

To be purchased from

York House, Kingsway, LONDON, W.C.2: 429 Oxford Street, LONDON, W.1
P.O. Box 569, LONDON, S.E.1

13a Castle Street, EDINBURGH, 2 | 1 St. Andrew's Crescent, CARDIFF
39 King Street, MANCHESTER, 2 | Tower Lane, BRISTOL, 1
2 Edmund Street, BIRMINGHAM, 3 | 80 Chichester Street, BELFAST

or from any Bookseller

PRINTED IN GREAT BRITAIN

1952

Price 8s. 0d. net

S.O. Code No. 23-9006-86